Journal of Archaeological Science: Reports 38 (2021) 103097

Contents lists available at ScienceDirect

Journal of Archaeological Science: Reports

journal homepage: www.elsevier.com/locate/jasrep

Geochemical changes in obsidian outcrops with elevation at Hatis volcano (Armenia) and corresponding Lower Palaeolithic artifacts from Nor Geghi 1

Ellery Frahm [a,*], Kristine Martirosyan-Olshansky [b], Jenni E. Sherriff [c], Keith N. Wilkinson [d], Phil Glauberman [e,f,g], Yannick Raczynski-Henk [h], Boris Gasparyan [f], Daniel S. Adler [i]

[a] Council on Archaeological Studies, Department of Anthropology, Yale University, United States
[b] Cotsen Institute of Archaeology, University of California-Los Angeles, United States
[c] Centre for Quaternary Research, Department of Geography, Royal Holloway, University of London, United Kingdom
[d] Department of Archaeology, Anthropology and Geography, University of Winchester, United Kingdom
[e] Department of Early Prehistory and Quaternary Ecology, University of Tübingen, Germany
[f] Institute of Archaeology and Ethnography, National Academy of Sciences, Armenia
[g] Xi'an Jiaotong-Liverpool University, Suzhou, China
[h] Human Origins Group, Leiden University, Netherlands
[i] Department of Anthropology, Archaeology Program, University of Connecticut, United States

ARTICLE INFO

Keywords:
Southern Caucasus
Armenian highlands
Pleistocene
Rhyolitic volcanism
Portable XRF
Obsidian sourcing
Geochronology

ABSTRACT

Most descriptions of obsidian-bearing rhyolitic lava flows and domes are largely based on relatively simple cases of tectonic plate subduction in North America, but Armenian geologists proposed since the 1960s that these models are less suitable for describing rhyolitic volcanism in their research area. Obsidian-producing volcanoes that lie in the Armenian Highlands, they argued, are more complex in form and stratification. Hatis volcano in central Armenia is one such example. As we document, Hatis is highly unusual, perhaps unique, in that its obsidian changes in composition with elevation. Prior studies of Hatis obsidian recognized the existence of two different chemical types. Here, though, we report a series of four obsidian chemical types and their spatial distributions across the slopes. Our findings were enabled by the use of portable XRF during our field surveys of Hatis. Additionally, we recognized each of these four chemical types of Hatis obsidian at the Lower Palaeolithic site of Nor Geghi 1, where thousands of obsidian artifacts reflect Pleistocene hominin behaviors from Marine Isotope Stage (MIS) 11 (~424–374 ka) to 9 (~337–300 ka). Thus, all four types of Hatis obsidian are archaeologically significant despite the fact that their outcrops span more than 500 m (from <1600 to greater than 2100 m asl) in elevation on the volcanic slopes, thereby enabling future studies on links between altitude and hominin toolstone acquisition behaviors over hundreds of millennia.

1. Introduction

The rise and development of obsidian sourcing in the Near East (Renfrew et al., 1966; 1968;; Dixon et al., 1968; Renfrew and Dixon, 1976) was influenced by geopolitical borders that existed until the end of the Cold War (Blackman, 1984; Keller et al., 1996). The border between Turkey and the Soviet Union quite literally shaped lasting concepts in the field of obsidian sourcing, from supply vs. contact zones to so-called "gravity models" of lithic source attractiveness. Hence, the abundance of obsidian in the Armenian Highlands (Fig. 1) went long unappreciated by Western archaeologists. For example, Renfrew et al. (1966) had only one obsidian specimen from what was then the Armenian Soviet Socialist Republic. Even in the 1990s, studies typically included just a few Armenian obsidian specimens with vague attributions (e.g., Gratuze et al., 1993; Bader et al., 1994; Hall and Shackley, 1994; Francaviglia and Palmieri, 1998). For example, Williams-Thorpe (1995) accurately discusses sources of obsidian across most of the Mediterranean region and Near East, but her map reveals the limits of Western knowledge about Armenian obsidian sources at the time. She put one star on her map near Yerevan for a supposed "Erevan" source and a second star near the northwestern tip of Lake Sevan for a "Sevan" source, neither of which is accurate. Such erroneous ideas about Armenian obsidian sources began to shift during the 2000s (e.g., Badalyan et al., 2004; Chataigner et al., 2003) and 2010s

* Corresponding author.
E-mail address: ellery.frahm@yale.edu (E. Frahm).

https://doi.org/10.1016/j.jasrep.2021.103097
Received 27 January 2021; Received in revised form 2 June 2021; Accepted 13 June 2021
Available online 24 June 2021

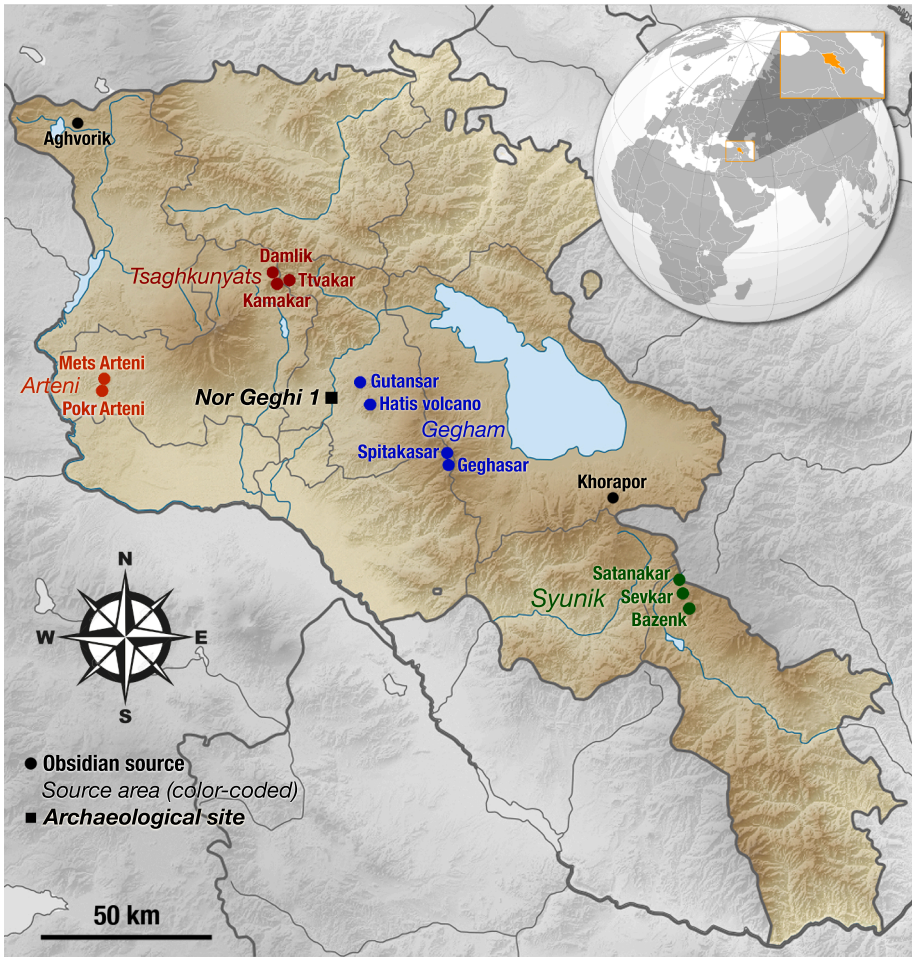

Fig. 1. Armenian obsidian sources (dots) and source complexes (color coded) as well as the Lower Palaeolithic site of Nor Geghi 1 (black square). The topographic map is based on digital elevation data from SRTM3 (Shuttle Radar Topography Mission dataset version 3).

Fig. 2. Northern side of Hatis volcano, as viewed from the southern slopes of Gutansar volcano (foreground), looking to the south, with the villages of Hatis to the left and Kaputan to the right.

(e.g., Cherry et al., 2010; Frahm, 2010, 2014; Chataigner and Gratuze, 2014; Martirosyan-Olshansky, 2014), after changing geopolitical conditions enabled more international collaborations with Armenian archaeological and geological research institutes. Additionally, a greater integration between geological field surveys of obsidian sources throughout the Armenian Highlands and the corresponding analytical work led to more nuanced understandings.

The same trend is also true with respect to the relevant geology. Descriptions and models of obsidian-producing rhyolitic volcanism have long been based on tectonically simple cases in North America (e.g.,

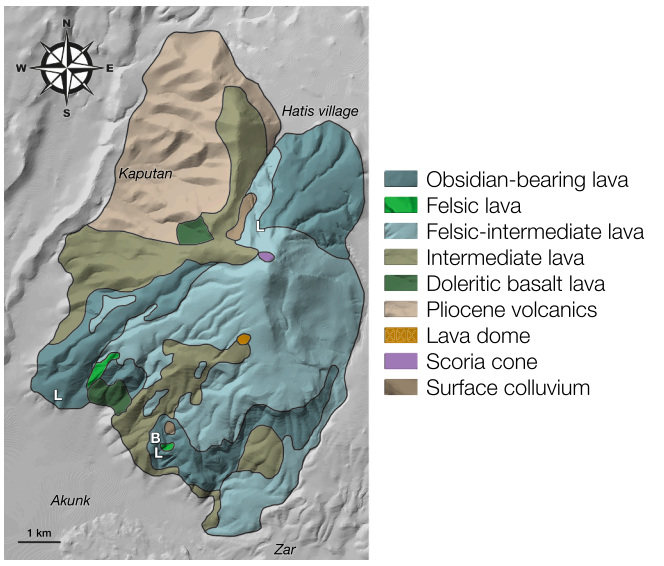

Fig. 3. Redrawn version of the Hatis geological map of Sherriff et al. (2019), largely based on that of Karapetian and Karapetian (1971). The only sampling location of Blackman et al. (1998) is demarked by a "B" on the map, and "L" marks the sampling locations of Lebedev et al. (2013).

Fink, 1980, 1987, 1994; Eichelberger et al., 1986; Fink and Manley, 1987; Hughes and Smith, 1993). For example, abundant obsidian sources throughout the Pacific Northwest, stretching from California to British Columbia, are the products of the oceanic Juan de Fuca Plate subducting beneath the continental North American Plate, creating silica-rich magma that led to rhyolitic lava flows and domes in the Cascade volcanic arc. Armenian geologists, though, have long noted that such simple models do not accurately describe volcanism within the Armenian Highlands (e.g., Shirinian and Karapetian, 1964), where the Arabian, Eurasian, Anatolian, and African plates interact (Reilinger et al., 1997). Shirinian and Karapetian (1964:26) note that, unlike rhyolitic lava domes elsewhere in the world, such "volcanoes of Armenia are represented by fan-like, stratified, and more complicated forms." Specifically, they point out that Hatis volcano is "a stratified edifice of considerable size, 1000 m high… [that is] very interesting from a petrological point of view" (26).

Since 2011, we have worked to include obsidian artifact sourcing as a routine component of Palaeolithic studies within the Armenian Highlands. An important aspect of this endeavor has been conducting the needed chemical analyses within Armenia using portable X-ray fluorescence (pXRF) instruments, and another is conducting surveys of the obsidian sources, including Hatis (Fig. 2), as we document here. In 2011, the first author visited Hatis with the late Sergey Karapetyan, who was, at the time, the Chief Researcher in the Volcanology Department of Armenia's Institute of Geological Sciences, National Academy of Sciences. As noted above, his research at Hatis dates back as far as the 1960s (Shirinian and Karapetian, 1964). During that 2011 visit, while standing in front of obsidian outcrops on the southernmost flanks of Hatis, he mentioned the existence of a different variety of obsidian farther up the slopes. His thought was that, rather than being autochthonous to Hatis, this other obsidian had been redeposited there by glaciers. Ultimately, our findings support a different interpretation, but his observation was crucial for initiating this line of research.

As we show here, Hatis volcano is highly unusual – perhaps even unique – in that its obsidian varies in composition with elevation. Previously published studies of Hatis obsidian recognized two different chemical types. However, as a result of our pXRF analyses of geological obsidian specimens at 80 sampling loci on the slopes of Hatis, here we document a sequence of four obsidian chemical types and their spatial distributions. This study was conducted as one part of our ongoing

Table 1
Elemental data from previously published studies involving Hatis obsidian.

reference	*technique*	*laboratory*	*names*	*n*	*Rb*		*Sr*		*Y*		*Zr*		*Nb*		*Fe*	
Keller & Seifried 1990	WDXRF	Freiburg	Hatis	1	106		113		18		91		20		6230	
Keller et al. 1996	WDXRF	Freiburg	Hatis A	2	107	± 1	113	± 1	19	± 1	87	± 6	20	± 1	6405	± 246
			Hatis B	2	93	± 7	204	± 41	18	± 1	125	± 21	20	± 1	11,235	± 1930
Blackman et al. 1998	NAA	NIST/Smithsonian	Hatis	5	126	± 5					149	± 9			6100	± 900
Lebedev et al. 2013	WDXRF	IGEM Russia	Phase I	1	105		127		14		106		19		9730	
			Phase II	1	107	± 6	122	± 18	15	± 3	102	± 6	21	± 4	11,270	± 495
Chataigner & Gratuze 2014	LA-ICP-MS	CNRS Orléans	Hatis 1	3	108	± 7	82	± 6	10	± 1	63	± 4	21	± 2	6184	± 924
			Hatis 2	1	92	± 8	134	± 7	10	± 1	86	± 6	20	± 1	9839	± 558

Table 2
Initial collection of Hatis geological obsidian specimens (Frahm 2010).

Specimen	Provenience	Observations	Location / notes
Correct source: Hatis obsidian			
AR.2009.7.1	M.J. Blackman	low Al-Ti cluster	unspecified location; specimen #ARO-008
AR.2009.7.2	M.J. Blackman	low Al-Ti cluster	unspecified location; specimen #ARO-008
AR.2009.8.1	M.J. Blackman	low Al-Ti cluster	unspecified location; specimen #ARO-009
AR.2009.8.2	M.J. Blackman	low Al-Ti cluster	unspecified location; specimen #ARO-009
AR.2009.27.1	I.P. Savov / J. F. Luhr	low Al-Ti cluster	unspecified location; field #9-31A-04
AR.2009.27.2	I.P. Savov / J. F. Luhr	low Al-Ti cluster	unspecified location; field #9-31A-04
AR.2009.28.1	I.P. Savov / J. F. Luhr	high Al-Ti cluster	unspecified location; field #9-31D-04
AR.2009.48.1	S.G. Karapetyan	high Al-Ti cluster	unspecified location; specimen #756d
AR.2009.72.2	R.S. Badalyan	high Al-Ti cluster	purportedly from the "Akunk deposit," apparently a lithic scatter
AR.2009.72.3	R.S. Badalyan	low Al-Ti cluster	purportedly from the "Akunk deposit," apparently a lithic scatter
AR.2009.73.1	R.S. Badalyan	low Al-Ti cluster	purportedly from the "Akunk deposit"
AR.2009.74.1	R.S. Badalyan	low Al-Ti cluster	purportedly from the "Zar deposit"
AR.2009.74.2	R.S. Badalyan	low Al-Ti cluster	purportedly from the "Zar deposit"
Incorrect source: Gutansar obsidian			
AR.2009.72.1	R.S. Badalyan	not Hatis obsidian	purportedly from the "Akunk deposit," apparently a lithic scatter
Incorrect source: Mets Arteni obsidian			
AR.2009.75.1	R.S. Badalyan	not Hatis obsidian	purportedly from the "Kaputan deposit," apparently a lithic scatter

research, including the Hrazdan Gorge Palaeolithic Project and the Pleistocene Archaeology, Geochronology, and Environment of the Southern Caucasus (PAGES) Project (see Sherriff et al., 2019). The Hrazdan River valley, adjacent to Hatis volcano, encompasses a cluster of sites that span the Lower through Upper Palaeolithic (see Gasparyan and Arimura, 2014; Sherriff et al., 2019 for overviews). One of the Lower Palaeolithic sites, Nor Geghi 1 (NG1), has a lithic assemblage that is entirely obsidian and reflects Pleistocene hominin behaviors between Marine Isotope Stage (MIS) 11 (~424–374 ka) and 9 (~337–300 ka; Adler et al., 2014). We show here that each chemical type of Hatis obsidian occurs among the NG1 lithics, highlighting that all four types are archaeologically significant despite the fact that the outcrops' elevations span more than 500 m on these volcanic slopes.

2. History of research on Hatis obsidian

Hatis (sometimes transliterated as "Atis" in earlier publications) is a Quaternary volcano on the western margins of the Gegham Range, a plateau composed of ~100 volcanic centers across an area of 2800 km^2 (Sherriff et al., 2019). The volcano reaches nearly 1000 m above its surroundings: its summit lies at 2530 m asl, and its base is 1450 m asl at Akunk village. Its eruptive stages are not particularly well dated (for various reasons, as discussed below); however, the currently available dates put the obsidian emplacement in the Middle Pleistocene, approximately half a million years ago. This obsidian- and perlite-bearing felsic stage was followed by eruptions of felsic-intermediate and intermediate lavas an unknown amount of time later (Fig. 3). The complex history of volcanism in the Gegham Range and along the Hrazdan River valley has recently been summarized by Sherriff et al. (2019), but it must be stressed that there is only a fragmentary framework for understanding these processes at present. This region experienced at least six phases of effusive volcanism during the Pleistocene, each of which included multiple intervals of volcanic activity, producing a series of interbedded lavas and sedimentary sequences, some of which contain artifacts. The archaeological focus of this study, NG1, is an example of a site contained in such sediments. As discussed in Section 5, NG1 has been well dated via ^{40}Ar–^{39}Ar dating and tephra analyses, but such detailed work has yet to be completed throughout the Gegham Range and its adjacent areas.

Studies of Hatis obsidian date to the 1960s and 1970s (e.g., Shirinian and Karapetian, 1964; Karapetian, 1966; 1968; 1970;; Karapetian and Karapetian, 1971), as do the first chronometric dates for Hatis obsidian. Fission track (FT) dating of Hatis obsidian produced an age of ~330 ka, but ^{40}K–^{40}Ar dating of the same material resulted in an age of ~650 ka (Komarov et al., 1972). It should be emphasized that similar inconsistencies between FT and ^{40}K–^{40}Ar dates occur for other obsidians in Armenia. For example, a specimen of obsidian from Gutansar volcano yielded a FT date of ~330 ka and a ^{40}K–^{40}Ar date of ~550 ka (Komarov et al., 1972). Therefore, there is a clear disparity between these two different dating techniques when applied to Armenian obsidian.

Keller and Seifried (1990) chemically analyzed a single obsidian specimen from Hatis using wavelength-dispersive XRF (WDXRF; Table 1), but within a few years, they had analyzed four Hatis obsidian specimens (Keller et al., 1996). Two compositions were noted among the specimens, which Keller et al. (1996) termed "A" and "B." Based on the elemental relationships between A and B obsidian, Keller and colleagues proposed the two obsidians had comagmatic origins, meaning that both likely derived from a common parent magma (rather than one of the types having originated elsewhere). Unfortunately, the spatial relationships of these four specimens – and the two obsidian chemical compositions – on the slopes of Hatis volcano were not elucidated.

Blackman et al. (1998) analyzed five obsidian specimens from the base of Hatis, near Akunk village (labeled as "B" in Fig. 3), using neutron activation analysis (NAA), and they found only one chemical composition of obsidian (Table 1). In the same volume, Poidevin (1998) noted, based on the data from Keller et al. (1996), that there are two distinct Hatis obsidian chemical types and that Sr, Rb, and Zr readily discern them. Unfortunately, instead of interpreting the considerable disparity between the FT and ^{40}K–^{40}Ar dates for Hatis obsidian in Komarov et al. (1972) as evidence that FT dates are unreliable, Poidevin (1998) speculates that "the two geochemical groups could match two totally separate periods of magmatic activity" (148): one period at 650 ka and a second one at 330 ka. Unfortunately, his specious idea that two Hatis obsidian compositions correspond to two vastly different eruptive periods still persists within the obsidian-focused literature.

Arutyunyan et al. (2007) refer to two volcanic phases at Hatis volcano: Phase I circa 700 ka and Phase II circa 500 ka. The two phases are based on three ^{40}K–^{40}Ar dates: 700 ± 30 ka and 660 ± 40 ka for two rhyolite specimens and 480 ± 40 ka for a single specimen of obsidian. Consequently, Arutyunyan et al. (2007) propose that there were two phases during which obsidian was produced at Hatis, but just one of the three specimens was reportedly obsidian. Unfortunately, their sampling locations at Hatis volcano are not reported, minimizing the value of their dates.

Lebedev et al. (2013) dated three obsidian specimens from Hatis volcano (the "L" locations in Fig. 3), and they also chemically analyzed these three specimens using WDXRF (Table 1). Their dates, they argue, imply two phases: Phase I circa 740 ± 250 ka ($n = 1$, note the 2σ uncertainty) and Phase II circa 480 ± 50 ka ($n = 2$). Due to small sample sizes and large uncertainties, these dates are not statistically significantly different. In addition, these obsidian specimens do not appear to differ geochemically (Table 1). Consequently, the proposed Phases I and II of Lebedev et al. (2013) do not correspond to the Hatis A and B obsidian compositions of Keller et al. (1996). As discussed later, it would

Table 3
Accuracy assessment based on five microbeam standards.

		SiO_2	TiO_2	Al_2O_3	Cr_2O_3	FeO_{tot}	MnO	MgO	CaO	Na_2O	K_2O	P_2O_5	F	SO_3	Cl
Smithsonian VG-568, USNM #72854: Rhyolitic obsidian, Yellowstone National Park															
Frahm 2010	mean	76.91	0.075	12.03	< LOD	1.122	0.022	0.030	0.433	3.68	5.01	< LOD	< LOD	< LOD	0.098
	st dev	0.35	0.009	0.10		0.110	0.008	0.005	0.016	0.15	0.08				0.011
Smithsonian recommended values															
Jarosewich et al. 1980		76.71	0.12*	12.06	< LOD	1.23	0.30	< 0.10	0.50	3.75	4.89	< 0.01	n.m.	n.m.	n.m.
Published values from the GeoReM Database															
Mean of database values	mean	76.84	0.08	12.24	< LOD	1.11	0.03	0.03	0.44	3.34	4.91	< LOD	0.17	< LOD	0.102
	st dev	0.46	0.01	0.24		0.05	0.01	0.01	0.04	0.46	0.09		0.04		0.009
Smithsonian VG-2, USNM #111240/52: Basaltic glass, Juan de Fuca Ridge															
Frahm 2010	mean	50.28	1.81	14.10	0.010	11.85	0.194	7.13	10.90	2.75	0.20	0.207	< LOD	0.356	0.035
	st dev	0.12	0.01	0.04	0.005	0.05	0.008	0.06	0.04	0.07	0.01	0.017		0.010	0.004
Smithsonian recommended values															
Jarosewich et al. 1980		50.81	1.85	14.06	< LOD	11.84	0.22	6.71	11.12	2.62	0.19	0.20	n.m.	n.m.	n.m.
Published values from the GeoReM Database															
Mean of published values	mean	50.66	1.93	13.88	0.016	11.88	0.21	6.76	11.00	2.67	0.22	0.221	0.05	0.355	0.031
	st dev	0.41	0.40	0.34	0.004	0.31	0.02	0.39	0.38	0.09	0.12	0.054	0.03	0.021	0.006
Smithsonian, USNM #113716: Basaltic glass, Indian Ocean															
Frahm 2010	mean	51.363	1.276	15.615	0.042	9.226	0.167	8.39	11.247	2.790	0.079	0.119	< LOD	0.256	< LOD
	st dev	0.177	0.015	0.113	0.003	0.061	0.012	0.18	0.040	0.109	0.004	0.013		0.014	
Smithsonian recommended values															
Jarosewich et al. 1980		51.52	1.30	15.39	< LOD	9.13	0.17	8.21	11.31	2.48	0.09	0.12	n.m.	n.m.	n.m.
Published values from the GeoReM Database															
Mean of published values	mean	51.45	1.38	15.22	n.m.	9.16	0.17	8.14	11.21	2.64	0.10	0.13	n.m.	0.29	n.m.
	st dev	0.01	0.08	0.06		0.11	0.01	0.03	0.11	0.01	0.03				
Smithsonian, USNM #2213: Tektite glass, synthetic, Corning Glass Company															
Frahm 2010	mean	75.23	0.507	11.25	< LOD	4.905	0.096	1.54	2.631	1.063	1.814	< LOD	< LOD	< LOD	0.013
	st dev	0.14	0.008	0.04		0.103	0.007	0.02	0.019	0.040	0.021				0.003
Smithsonian recommended values															
Jarosewich et al. 1980		75.75	0.50	11.34	< LOD	4.96	0.11	1.51	2.66	1.06	1.88	< LOD	n.m.	n.m.	n.m.
Published values from literature sources															
Mean of published values	mean	75.85	0.51	11.20	n.m.	4.96	0.10	1.53	2.66	0.99	1.94	n.m.	n.m.	n.m.	n.m.
	st dev	0.92	0.01	0.15		0.10	0.01	0.05	0.06	0.01	0.07				
G-Probe-2/USGS NKT-1G: Peralkaline basaltic glass, Knippa, Texas															
Frahm 2010	mean	38.60	3.96	10.35	n.m.	12.36	0.19	14.79	13.43	3.33	1.38	0.95	n.m.	n.m.	n.m.
	st dev	0.18	0.07	0.09		0.12	0.02	0.63	0.11	0.06	0.03	0.07			
Interlaboratory "round robin" in Potts et al. (2005)															
Recommended values	mean	38.68	3.95	10.20	0.06	12.11	0.21	14.33	13.21	3.48	1.28	0.97	n.m.	n.m.	n.m.
	st dev	0.07	0.01	0.04	0.01	0.05	0.01	0.05	0.04	0.02	0.01	0.02			

* Known error: mean published values compiled in the GeoReM Database all fall between 0.05% and 0.09%
< LOD: Below minimum limits of detection
n.m.: Not measured

be highly unusual for two obsidian-bearing flows to vary so greatly in time (e.g., hundreds of millennia) but not in trace-element composition. Instead, the two proposed phases seem to reflect the considerable measurement uncertainty (2σ of ± 250 ka) of their Phase I date.

Citing Arutyunyan et al. (2007), Chataigner and Gratuze (2014:38) write that, at Hatis, "two phases of activity have been recognized: (a) approximately 700 ka ago, the formation of the Hatis volcano – the composition of the obsidian corresponds to calc-alkaline rhyolites [and] (b) about 50 ka ago." Note that the second date reflects either a typographical error or misreading of Arutyunyan et al. (2007), who proposed a volcanic phase at Hatis circa 500 (not 50) ka. Chataigner and Gratuze (2014:38) conclude a discussion of Hatis, including laser ablation inductively coupled plasma mass spectrometry (LA-ICP-MS) measurements of four obsidian specimens, as follows:

> Poidevin (1998) has distinguished three subgroups: Hatis I and Hatis II belong to the first phase of activity; while Hatis III, a vitreous rhyolite enriched in rare earth elements, belongs to the second phase… The obsidian from the Hatis mountain is represented by two groups that are easily differentiated by their strontium content. The first one (Hatis 1), with lower strontium concentrations (about 81 ppm), originates in the western outcrops (Akunk *[2 specimens]* and Kaputan *[1 specimen]*), while the second one (Hatis 2), with higher strontium contents (136 ppm), comes from the southeastern slopes (Zerborian *[1 specimen; perhaps named after the village of Zar]*). (brackets and italics added)

Four observations can be made about this paragraph. First, as previously noted, Poidevin's (1998) speculative phases were based on a disparity between FT and ^{40}K–^{40}Ar dates for the same material, not different compositions of Hatis obsidian. Second, Poidevin (1998) makes no mention of a "Hatis III" vitreous rhyolite (although we located an aphanitic trachyte on Hatis that might be the material in question; Frahm, 2019). Third, the spatial distributions are vague and simply named for nearby villages. Lastly, Chataigner and Gratuze (2014) report lower Sr values for their Hatis 1 and 2 (81 and 136 ppm, respectively) than do Keller et al. (1996) for Hatis A and B obsidians (113 and 204 ppm; Table 1), complicating the question of whether the Hatis 1 and 2 obsidians are equivalent to Hatis A and B obsidians. There are, though, known offsets between their LA-ICP-MS data (including Sr) and other published values for Armenian obsidians (Frahm, 2014). For example, they list a Sr content of 87 ± 12 ppm for Gutansar obsidian, but an inter-laboratory comparison resulted in a recommended Sr value of 129 ± 6 ppm (Frahm, 2019). Likewise, for Aghvorik obsidian, they report a Sr content of 143 ± 6 ppm, but the recommended inter-laboratory value for Sr is 198 ± 9 ppm (Frahm, 2019). As a result, it is challenging to directly correlate "Hatis A and B" (Keller et al., 1996) with "Hatis 1 and 2" (Chataigner and Gratuze, 2014), even if it would seem logical to simply do so.

Perhaps most importantly, the elemental data for Hatis obsidian reported by Chataigner and Gratuze (2014) were first published in Gratuze (2007), in which it was evident that these obsidian specimens derived from archaeological lithic scatters, not geological outcrops. Gratuze (2007) does not specify how or when the purported geological specimens were collected. It is telling, however, that he identified Gutansar obsidian at two of the Hatis sampling locations (Kaputan and Zovashen) as well as Hatis obsidian at one of the Gutansar sampling locations (Fontan). This is a common issue with secondhand specimens from the Armenian Highlands, where lithic scatters composed entirely of obsidian artifacts frequently occur on this complex volcanic landscape. For example, Blackman (1984) reported two different obsidian compositions ("Sevan I," $n = 5$ and "Sevan II," $n = 1$) among six specimens from a purported "Lake Sevan" obsidian source. Instead, his data suggest that "Sevan I" corresponds to Gutansar and "Sevan II" corresponds to Geghasar obsidian, which would be consistent with an archaeological lithic scatter expected in such a location. Ultimately, though, Gratuze (2007) recognized that these Hatis and Gutansar obsidian samples were mixed, and the admixture was not his fault. It means, however, that the location descriptions lack geological relevance.

3. Authors' preliminary research

The first two authors conducted studies of Hatis obsidian during the course of their doctoral dissertations (Frahm, 2010; Olshansky, 2018; see also Martirosyan-Olshansky, 2014). Their findings and datasets based on various analytical techniques are summarized below.

3.1. Frahm's data and findings

Frahm (2010) assembled an initial collection of Hatis obsidian thanks to specimens from (1) M. James Blackman (see Section 2 above and Blackman et al., 1998) of the Smithsonian Institution's Nuclear Laboratory for Archaeological Research; (2) James Luhr from the Global Volcanism Project of the Smithsonian's National Museum of Natural History and his former postdoctoral researcher, Ivan Savov; (3) our friend and colleague Sergey Karapetyan (e.g., Karapetian et al, 2001); and (4) Ruben Badalyan (e.g., Badalyan et al., 2004) from the Institute of Archaeology and Ethnography, National Academy of Science, Republic of Armenia. The details regarding this initial collection are summarized in Table 2. Of the fifteen assembled obsidian specimens, thirteen derived from Hatis, whereas the other two originated from different obsidian sources. These two specimens (one from Gutansar, one from Mets Arteni) likely reflect, at least in part, the same issue encountered by Gratuze (2007): sampling from anthropogenic lithic scatters, not geological outcrops.

3.1.1. EMPA at the University of Minnesota

All of these obsidian specimens were chemically analyzed with electron microprobe analysis (EMPA), specifically a JEOL 8900R housed in the Department of Earth and Environmental Sciences, University of Minnesota. EMPA is a variety of X-ray spectrometry that not only has been used for sourcing obsidian artifacts for three decades (e.g., Merrick and Brown, 1984a; 1984b;; Merrick et al., 1994; Tykot, 1997) but also is favored by tephrochronologists to geochemically match volcanic ash to a given eruption (e.g., Smith et al., 1977; Tryon et al., 2009). Fourteen "major" elements (e.g., Si, Ti, Al, Fe, Mn, Ca, Na, K) were measured under a set of conditions (15 kV voltage, 60 nA current, 30 μm beam diameter, 25 s each on peak and background measurements) that minimized beam-induced alteration in obsidian (e.g., Na and K migration; Hunt and Hill, 2001). Other special procedures (e.g., periodic re-peaking of the spectrometers) are documented by Frahm (2012). Data correction used JEOL's implementation of the ZAF scheme, and calibration relied on microbeam standards from the Smithsonian (e.g., Kakanui hornblende for Mg, Ca, Ti, Fe) and elsewhere.

Accuracy of the EMPA measurements was assessed using five microbeam glass standards as well as a well-characterized obsidian specimen. Table 3 summarizes the EMPA measurements and published values for the five standards: (1) Smithsonian VG-568, USNM #72854: rhyolitic obsidian, Yellowstone National Park; (2) Smithsonian VG-2, USNM #111240/52: basaltic glass, Juan de Fuca Ridge; (3) Smithsonian, USNM #113716: basaltic glass, Indian Ocean; (4) Smithsonian, USNM #2213: tektite glass, synthetic, Corning Glass; and (5) G-Probe-2/USGS NKT-1G: peralkaline basaltic glass, Knippa, Texas. The EMPA measurements compare well to values from the Smithsonian Microbeam Standards program (Jarosewich et al., 1980), the G-Probe-2 testing program (Potts et al., 2005), and the GeoReM (Geological and Environmental Reference Materials) web database. Table 4 shows the EMPA measurements and inter-laboratory values (Glascock, 1999; Frahm, 2019) for a specimen of Sierra de Pachuca (Mexico) obsidian, which has essentially become a de facto standard for sourcing. The datasets exhibit excellent agreement and, thus, high accuracy. Table 5 lists the EMPA data for these Hatis specimens, which, when plotted, reveal two clusters (Fig. 4).

Table 4
Interlaboratory data comparison for Sierra de Pachuca obsidian.

Technique	Laboratory	Publication		SiO_2	TiO_2	Al_2O_3	Cr_2O_3	FeO_{tot}	MnO	MgO	CaO	Na_2O	K_2O	P_2O_5	F	SO_3	Cl
Sierra de Pachuca specimen analyzed by the first author																	
EMPA	University of Minnesota	Frahm 2010	mean	75.70	0.19	11.30	< LOD	2.17	0.14	0.05	0.11	5.02	4.63	< LOD	< LOD	< LOD	0.19
			st dev	0.36	0.01	0.07		0.03	0.01	0.01	0.02	0.30	0.09				0.01
Mean values derived from published datasets below																	
			mean	75.98	0.20	11.68	n.m.	2.13	0.14	0.07	0.12	5.26	4.42	0.03	0.29	n.m.	0.14
			st dev	2.94	0.03	0.90		0.14	0.02	0.04	0.03	0.35	0.43	0.02	0.02		0.02
Published datasets for Sierra de Pachuca obsidian																	
EDXRF	Ashe Analytics, Montana	Glascock 1999	mean					2.11	0.14								
			st dev					0.14	0.01								
	Geoarchaeological XRF Lab	Silva de la Mora 2018	mean		0.23			2.44	0.13								
			st dev		0.01			0.07	0.01								
	MURR Archaeometry Lab	Frahm 2019						2.01	0.13								
		Glascock 2011	mean		0.16			2.05	0.10				4.60				
			st dev		0.02			0.15	0.01				0.20				
	NWR Obsidian Studies Lab	Glascock 1999	mean		0.19			2.21	0.15								
			st dev		0.02			0.08	0.01								
ICP-AES/MS	CNRS, Grenoble, France	Glascock 1999	mean			10.43		1.96	0.16	0.05	0.10	5.28	3.75	0.01			
			st dev			0.40		0.08	0.01	0.01	0.01	0.09	0.08				
	PUC–Rio de Janeiro, Brazil	Glascock 1999			0.18	12.32		2.14	0.11	0.06	0.09	5.27	4.44				
ICP-MS	PUC–Rio de Janeiro, Brazil	de B. Pereira et al. 2001	mean		0.18				0.11								
			st dev		0.01				0.01								
	MURR Archaeometry Lab	Glascock & Ferguson 2012		76.85	0.19	11.50		1.99	0.15	0.07	0.11	5.20	4.50				
LA-ICP-MS	CNRS, Orléans, France	Glascock 1999	mean	75.30	0.20	12.30		2.21	0.14	0.05	out	5.10	4.17	0.04			
			st dev	0.21	0.01	0.42		0.13	0.01	0.01		0.23	0.04				
	California State University	Carballo et al. 2007	mean					2.10	0.14			5.01	4.32				
			st dev					0.10	0.01			0.30	0.20				
	PUC–Rio de Janeiro, Brazil	de B. Pereira et al. 2001	mean		0.23				0.13								
			st dev		0.01				0.01								
	MURR Archaeometry Lab	Glascock & Ferguson 2012		72.72	0.25	13.41		2.18	0.13	0.05	0.15	5.28	5.33				
NAA	CNRS, Orléans, France	Glascock 1999	mean	73.38	0.22	11.70		2.21	0.13	out	0.16	6.00	5.10				
			st dev	0.64	0.01	0.08		0.13	0.02		0.03	0.54	0.07				
	MURR Archaeometry Lab	Frahm 2019				11.57		2.07	0.14			4.98	3.99				0.12
		Cobean et al., 1991	mean					1.99	0.14			5.01	4.76				0.15
			st dev					0.13	0.02			0.19	0.36				0.03
		Glascock 1999	mean					2.03	0.15			5.12	4.55				0.15
			st dev					0.03	0.01			0.12	0.29				0.02
		Glascock & Ferguson 2012				11.48		2.09	0.14			5.01	3.96				0.11
PIXE	CNRS, Grenoble, France	Glascock 1999	mean	76.37	0.18	10.43		2.01	0.13		0.11	5.16	4.08				0.16
			st dev	0.11	0.01	0.40		0.03	0.01		0.01	0.11	0.04				0.01
PIXE/PIGME	ANSTO, Australia	Glascock 1999	mean	81.72	0.19	12.41		2.33	0.16		0.13	6.11	4.61		0.29		
			st dev	4.28	0.01	0.66		0.15	0.01		0.01	0.36	0.20		0.02		
WDXRF	CNR-ITABC, Rome, Italy	Glascock 1999		75.52	0.21	10.92		2.43	0.15	0.14	0.11	5.04	4.18				

out: Extreme outlier measurement removed from the data table due to clear analytical errors
< LOD: Below minimum limits of detection
n.m.: Not measured

Table 5
EMPA measurements of the initial Hatis geological obsidian specimens.

Specimen / source		SiO_2	TiO_2	Al_2O_3	Cr_2O_3	FeO_{tot}	MnO	MgO	CaO	Na_2O	K_2O	P_2O_5	F	SO_3	Cl
Correct source: Hatis obsidian															
AR.2009.7.1	mean	75.64	0.101	13.87	< LOD	0.838	0.060	0.158	0.991	4.304	4.325	0.020	< LOD	< LOD	0.044
	std dev	0.15	0.006	0.06		0.019	0.011	0.005	0.034	0.176	0.032	0.008			0.006
AR.2009.7.2	mean	75.46	0.101	13.87	< LOD	0.834	0.059	0.152	1.014	4.310	4.310	0.021	< LOD	< LOD	0.048
	std dev	0.21	0.010	0.07		0.019	0.010	0.007	0.019	0.177	0.048	0.012			0.005
AR.2009.8.1	mean	75.14	0.103	13.81	< LOD	0.840	0.062	0.156	0.978	4.331	4.341	0.023	0.004	< LOD	0.045
	std dev	0.24	0.007	0.05		0.021	0.007	0.007	0.011	0.148	0.022	0.008	0.003		0.006
AR.2009.8.2	mean	75.51	0.101	13.90	< LOD	0.856	0.060	0.157	0.968	4.369	4.291	0.017	< LOD	< LOD	0.048
	std dev	0.30	0.008	0.05		0.015	0.007	0.007	0.022	0.117	0.043	0.011			0.006
AR.2009.27.1	mean	75.50	0.101	13.82	< LOD	0.408	0.052	0.088	0.951	4.319	4.316	0.021	< LOD	< LOD	0.042
	std dev	0.28	0.008	0.16		0.029	0.008	0.015	0.073	0.144	0.080	0.009			0.007
AR.2009.27.2	mean	75.23	0.104	13.82	< LOD	0.420	0.052	0.087	0.953	4.281	4.365	0.022	< LOD	< LOD	0.047
	std dev	0.23	0.008	0.13		0.029	0.011	0.016	0.020	0.131	0.070	0.009			0.005
AR.2009.28.1	mean	74.83	0.145	14.15	< LOD	0.594	0.050	0.188	1.159	4.302	4.333	0.047	< LOD	< LOD	0.045
	std dev	0.39	0.009	0.12		0.132	0.011	0.084	0.112	0.098	0.112	0.008			0.006
AR.2009.48.1	mean	74.76	0.130	14.13	< LOD	0.868	0.050	0.167	1.082	4.018	4.839	0.032	< LOD	< LOD	0.044
	std dev	0.26	0.007	0.03		0.079	0.011	0.033	0.050	0.131	0.069	0.008			0.006
AR.2009.72.2	mean	74.51	0.128	14.07	< LOD	0.671	0.052	0.230	1.205	4.241	4.297	0.034	< LOD	< LOD	0.051
	std dev	0.20	0.007	0.08		0.072	0.008	0.018	0.028	0.126	0.054	0.008			0.023
AR.2009.72.3	mean	74.87	0.089	13.80	< LOD	0.735	0.062	0.126	0.848	4.181	4.557	0.013	< LOD	< LOD	0.049
	std dev	0.15	0.008	0.05		0.062	0.007	0.013	0.095	0.179	0.091	0.006			0.005
AR.2009.73.1	mean	75.52	0.100	13.70	< LOD	0.846	0.054	0.151	0.980	4.235	4.299	0.025	< LOD	< LOD	0.049
	std dev	0.29	0.012	0.34		0.010	0.010	0.008	0.009	0.168	0.029	0.009			0.009
AR.2009.74.1	mean	74.92	0.092	13.79	< LOD	0.633	0.059	0.151	0.948	4.237	4.393	0.018	< LOD	0.011	0.042
	std dev	0.18	0.008	0.07		0.087	0.013	0.006	0.034	0.110	0.067	0.008		0.007	0.006
AR.2009.74.2	mean	74.71	0.092	13.78	< LOD	0.822	0.058	0.151	0.942	4.237	4.373	0.022	< LOD	0.014	0.044
	std dev	0.16	0.007	0.10		0.019	0.006	0.007	0.035	0.136	0.049	0.006		0.009	0.005
Incorrect source: Gutansar obsidian															
AR.2009.72.1	mean	74.61	0.159	13.93	< LOD	0.546	0.057	0.201	0.993	4.355	4.446	0.033	< LOD	< LOD	0.028
	std dev	0.21	0.009	0.15		0.098	0.010	0.010	0.030	0.107	0.048	0.014			0.007
Gutansar data	mean	74.55	0.175	14.00	< LOD	0.947	0.073	0.189	0.971	4.415	4.256	0.033	0.003	0.004	0.038
	std dev	0.40	0.003	0.12		0.238	0.008	0.041	0.033	0.070	0.086	0.003	0.001	0.002	0.003
Incorrect source: Mets Arteni obsidian															
AR.2009.75.1	mean	76.84	0.062	13.46	< LOD	0.455	0.096	0.039	0.492	4.470	4.360	< LOD	< LOD	< LOD	0.041
	std dev	0.22	0.007	0.05		0.017	0.008	0.005	0.014	0.140	0.141				0.008
Mets Arteni data	mean	76.40	0.059	13.23	< LOD	0.362	0.092	0.035	0.487	4.115	4.797	0.006	< LOD	< LOD	0.042
	std dev	0.02	0.003	0.06		0.020	0.003	0.006	0.010	0.039	0.096	0.002			0.002

< LOD: Below minimum limits of detection

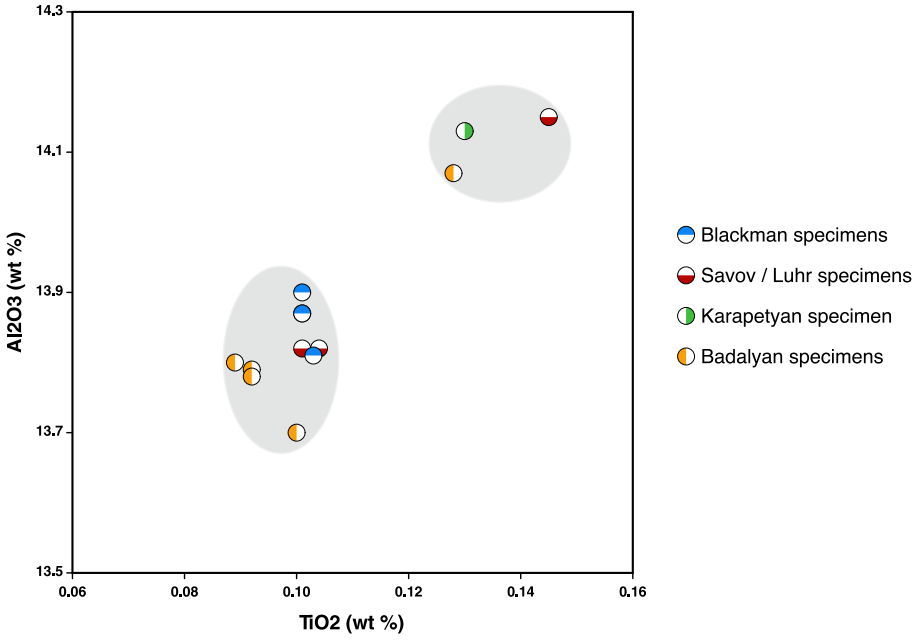

Fig. 4. Scatterplot of TiO_2 vs. Al_2O_3, as measured via EMPA, for the initial Hatis obsidian specimens, revealing the presence of two chemical types among these specimens.

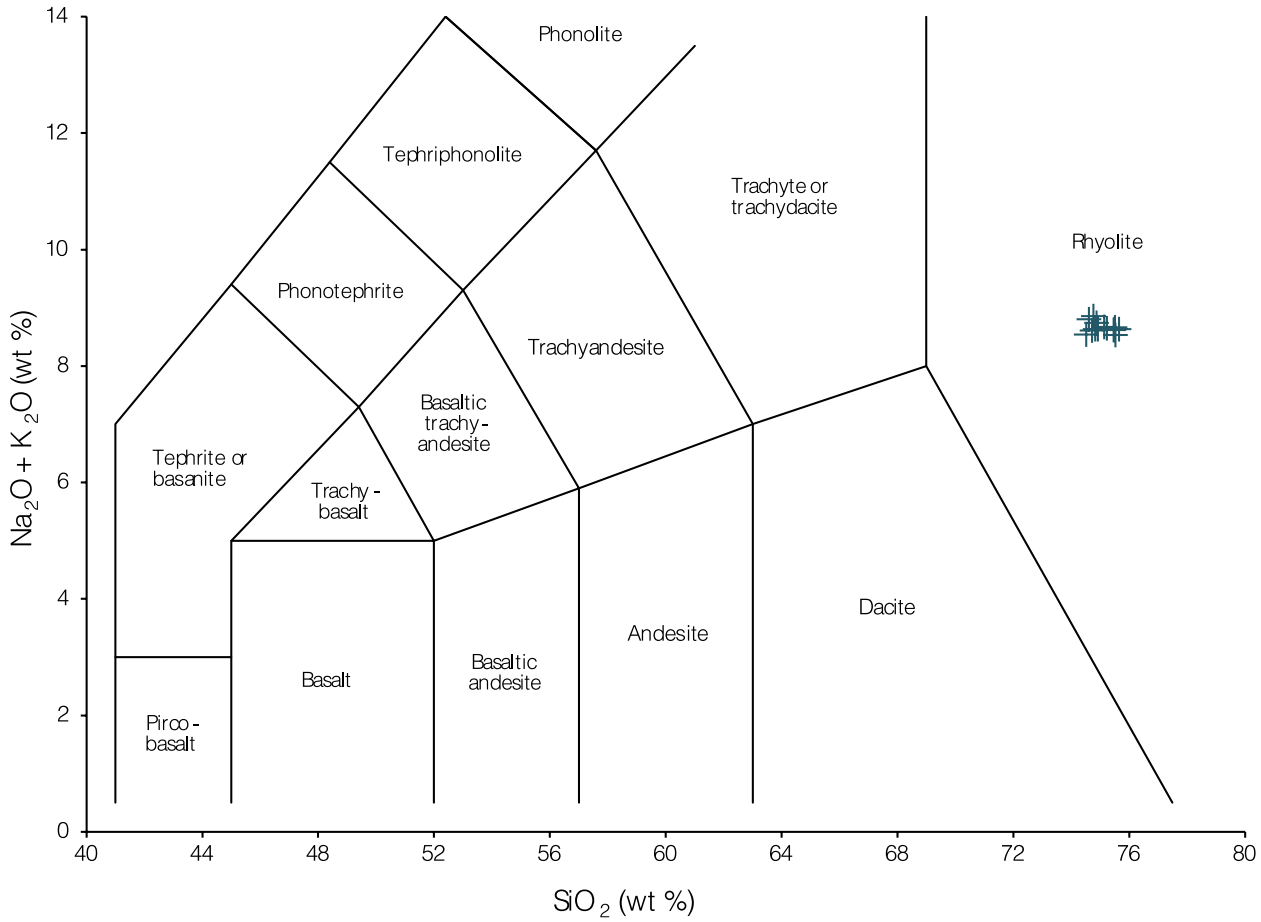

Fig. 5. Plot of the EMPA data for the Hatis obsidian specimens on a TAS (Total Alkali Silica) diagram (Le Maitre et al., 2002), demonstrating that, as anticipated, they are rhyolitic in composition.

These EMPA data are important for several reasons. First, thirteen Hatis obsidian specimens were, at the time, the largest available dataset for this volcano (e.g., Blackman et al., 1998 tested five specimens). Second, the results show how the four obsidian types at the volcano went unnoticed for so long. As attested by obsidian that derived from other volcanoes (Gutansar and Mets Arteni), some portion of the specimens likely came from anthropogenic lithic scatters rather than outcrops. Third, these data allow us to plot the Hatis specimens on a TAS (Total Alkali Silica) diagram (Le Maitre et al., 2002). All of the specimens fall together, as expected, in the "rhyolite" portion of this diagram (Fig. 5). Finally, based on Student's *t* tests, six elements within the EMPA dataset have statistically different concentrations between these two chemical types of Hatis obsidian: SiO_2 ($p = 0.0188$), TiO_2 ($p < 0.0001$), Al_2O_3 ($p < 0.0001$), MnO ($p = 0.0097$), MgO ($p = 0.0115$), and CaO ($p < 0.0001$). Nevertheless, the two types of Hatis obsidian seem to be comagmatic, consistent with Keller et al. (1996).

3.1.2. NAA and EDXRF at MURR

Some of the obsidian specimens were sent to the Archaeometry Laboratory at the University of Missouri Research Reactor (MURR) for NAA and energy-dispersive XRF (EDXRF), as discussed by Frahm (2010). For NAA, obsidian specimens were crushed to yield small fragments for two rounds of irradiation, as described by Glascock (1999). For the short irradiation, 100 mg of fragments were exposed to a neutron flux for 5 s, and they sat idle for 25 min before the emitted gamma rays were measured for 12 min. In the long irradiation, 300 mg of fragments were irradiated for 70 h and then measured twice: a 2000-second measurement took place after eight days, and a three-hour measurement took place after another four weeks. These measurements were calibrated using the United States' National Institute of Standards and Technology (NIST) standard #278 (an obsidian reportedly from Newberry Caldera, Oregon), and NIST standard #1633a (trace elements in bituminous coal fly ash) was used as a quality check of the data. The resulting measurements for 28 elements are summarized in Table 6. Several other obsidian specimens tested at the same time are now included within the Peabody–Yale Reference Obsidians (PYRO) calibration and evaluation sets (Frahm, 2019), so Table 7 gives a comparison to assess the accuracy.

Obsidian specimens were also analyzed at MURR with an ElvaX EDXRF system, as described by Glascock (2011). This instrument is equipped with a 5-W X-ray tube (W anode, 50 kV maximum voltage, 100 μA maximum current) and a Si P-N diode detector with an energy resolution of 180 eV in practice. Eleven elements of interest (K, Ti, Mn, Fe, Zn, Ga, Rb, Sr, Y, Zr, Nb) were measured with a voltage of 40 kV and a current set to yield a count rate of ~6000 cps. The specimens were measured whole (i.e., without preparation as powders), and the X-ray beam diameter was ~3–4 mm. Each was measured for 3–5 min. The resulting spectra were downloaded to a PC for peak deconvolution and quantification using proprietary software. Their standards were a set of 40 obsidian specimens which were drawn from the MURR collections (and which became a basis for the Bruker "obsidian" calibration for Tracer pXRF models; Glascock and Ferguson, 2012). Table 8 summarizes the EDXRF data for the Hatis obsidian specimens. As with NAA, several specimens concurrently measured with EDXRF are included in PYRO sets (Frahm, 2019), and Table 7 also shows a comparison to the interlaboratory recommended values to evaluate the EDXRF data accuracy.

Table 9 establishes that, for elements in common between NAA and EDXRF, there are a few statistically significant differences between the two datasets, as determined using a Student's *t* test. For example, as

Table 6
NAA measurements at MURR of the initial Hatis geological specimens.

Source / specimen	Ba	La	Lu	Nd	Sm	U	Yb	Ce	Co	Cs	Eu	Fe	Hf	Rb	Sb	Sc	Sr	Ta	Tb	Th	Zn	Zr	Al	Cl	Dy	K	Mn	Na
Correct source: Hatis obsidian																												
AR.2009.48.1	522	28	0.3	13	3	9	2	48	1.2	4	0.5	7575	3	106	0.3	2	183	2	0.4	17	33	77	73,454	258	2	30,184	493	33,047
AR.2009.72.2	556	29	0.3	14	3	9	2	48	1.2	4	0.5	7902	3	104	0.3	2	181	2	0.4	16	37	79	78,928	293	3	35,223	507	32,333
AR.2009.72.3	540	27	0.3	14	3	9	2	46	0.7	5	0.5	6304	3	113	0.4	2	142	2	0.4	17	36	70	74,898	309	2	34,783	493	31,661
AR.2009.73.1	516	27	0.3	13	3	10	2	46	0.6	4	0.5	6219	3	112	0.3	2	143	2	0.4	17	37	67	77,606	329	3	35,530	507	32,224
Incorrect source: Mets Arteni obsidian																												
AR.2009.75.1	38	11	0.5	8	4	9	3	25	0.0	4	0.2	3359	3	146	0.5	3	15	3	0.7	14	45	30	73,643	230	5	36,402	753	31,962
Mets Arteni means	28	11	0.5	9	4	8	3	26	0.1	4	0.2	3389	3	148	0.5	3	–	3	0.7	15	46	41	72,180	256	5	36,977	748	30,582

corroborated by Table 7, the EDXRF measurements for Zr are more accurate than the NAA measurements, but the reverse is true for Mn (i.e., the NAA data are more accurate). Three useful observations can, nevertheless, be made from these two datasets. First, the data confirm that two of the "Hatis" obsidian specimens originated from other sources (i.e., Gutansar and Mets Arteni), perhaps due to sampling from lithic scatters. Second, these data also confirm the occurrence of two chemical clusters among the actual Hatis specimens. Third, the datasets can reveal which elements exhibit statistically significant differences between the Hatis clusters, even though the sample sizes are small ($n = 6$ for EDXRF, $n = 4$ for NAA). Using a Student's t test, five elements in the EDXRF data have statistically significant differences between the two clusters: Ti ($p = 0.0062$), Fe ($p = 0.0011$), Zn ($p = 0.0069$), Sr ($p = 0.0094$), and Zr ($p = 0.0376$). In addition, Rb lies on the cusp of significance ($p = 0.0778$). Among the NAA data, four elements are significantly different and have concentrations in Hatis obsidian above the minimum detection limits of newer pXRF instruments: Fe ($p = 0.0128$), Rb ($p = 0.0215$), Sr ($p = 0.0008$), and Zr ($p = 0.0342$). Given these compositional differences between clusters in the EDXRF and NAA data, we focus on Fe, Rb, Sr, and Zr for this study.

3.2. *Martirosyan-Olshansky's data and findings*

Independently, Martirosyan-Olshansky visited and sampled a number of Armenian obsidian sources, including Hatis volcano, in 2013. Specifically, she collected 16 obsidian specimens from the southwestern slopes of Hatis volcano above the village of Akunk, and she transported them back to the University of California-Los Angeles (UCLA) for elemental analysis and chemical comparison to artifacts from the Neolithic settlement of Masis Blur (Martirosyan-Olshansky, 2014). At UCLA, she used a Bruker Tracer III-V+ pXRF instrument (a Rh anode, Si PIN-diode detector with a resolution of ~190 eV at a count rate of 10,000 cps) with their typical protocols for obsidian analysis (voltage: 40 kV, current: 14 μA, Cu-Ti beam filter, 200 s measurements). For quantification, the instrument used the MURR/Bruker "obsidian" calibration scheme, and three standards from the United States Geological Survey (USGS) – AGV-1 (andesite, Gunao Valley, Oregon), SCo-1 (Cody Shale, Teapot Dome, Wyoming), and QLO-1a (quartz latite, Lake County, Oregon) – were also analyzed to assess accuracy. Among the 16 Hatis specimens, she identified two chemical types, which she termed "Akunq A" and "Akunq B" (Martirosyan-Olshansky, 2014), and Table 10 includes the corresponding values. Based on her Sr data, which exhibited very low error (2–3% relative) for the USGS standards, Akunq A and B seem to correspond to Hatis A and B, respectively, in Keller et al. (1996).

Later in her dissertation research, she added 16 new obsidian specimens from the northern, eastern, and southeastern slopes of Hatis volcano to her initial dataset (Olshansky, 2018). Using the same pXRF instrument with the additional specimens, she identified four chemical types from Hatis that are best differentiated by the Fe, Sr, and Zr concentrations, as shown here in Table 10, and as a result, she devised a new naming system in light of the newly recognized obsidian types (i.e., Akunq A became Hatis 1, Akunq B became Hatis 3). That is, her insights into the complexity of Hatis as an obsidian source were a direct result of conducting more extensive surveys and sampling across the volcano than those who preceded her, as documented here in Section 2.

4. Refining the obsidian types at Hatis

The following sections report the results from our pXRF analyses at 80 sampling loci across Hatis volcano. This method allowed us to recognize and map out the four obsidian types in the field, and we discuss our interpretations of these data and the current limitations.

Table 7
Assessment of the EDXRF and NAA measurements at MURR.

Specimen / dataset	Mn			Fe			Zn			Rb			Sr			Y			Zr			Nb		
Aghvorik obsidian (Armenia)																								
inter-laboratory data	472	±	24	12,240	±	690	48	±	4	98	±	5	198	±	9	15	±	6	236	±	15	18	±	4
EDXRF measured values	439	±	51	10,349	±	170	53	±	1	94	±	2	230	±	5	11	±	1	229	±	5	14	±	1
NAA measured values	490	±	7	12,100	±	53	48	±	2	99	±	1	216	±	12	n.m.			229	±	17	n.m.		
Gutansar obsidian (Armenia)																								
inter-laboratory data	641	±	23	8250	±	173	44	±	4	140	±	5	129	±	6	22	±	7	171	±	13	37	±	3
EDXRF measured values	524	±	38	7642	±	198	50	±	3	144	±	3	136	±	5	11	±	3	180	±	5	31	±	2
NAA measured values	636	±	8	8173	±	240	42	±	2	140	±	1	129	±	13	n.m.			138	±	15	n.m.		
Satanakar obsidian (Armenia)																								
inter-laboratory data	522	±	20	4580	±	180	34	±	2	192	±	2	9	±	2	8	±	4	88	±	10	36	±	3
EDXRF measured values	341			5066			28			186			10			1			89			28		
NAA measured values	535	±	23	4333	±	143	34	±	1	192	±	5	< LOD			n.m.			41	±	12	n.m.		
Chikiani 1 obsidian (Georgia)																								
inter-laboratory data	482	±	40	5000	±	280	41	±	4	130	±	7	75	±	12	14	±	4	81	±	4	19	±	2
EDXRF measured values	372	±	36	5975	±	336	38	±	2	130	±	5	94	±	10	9	±	3	97	±	8	18	±	3
Meydan Dağ obsidian (Turkey)																								
inter-laboratory data	519	±	27	9520	±	310	74	±	8	200	±	5	18	±	3	52	±	5	286	±	15	32	±	4
EDXRF measured values	416	±	40	8877	±	190	65	±	3	192	±	3	17	±	3	51	±	2	277	±	12	29	±	3
NAA measured values	541			9616			75			203			< LOD			n.m.			262			n.m.		
Nemrut Dağ 6 obsidian (Turkey)																								
inter-laboratory data	1380	±	18	46,680	±	3860	237	±	10	233	±	8	2	±	1	145			1308	±	82	76	±	9
EDXRF measured values	1597	±	274	43,917	±	3630	250	±	21	231	±	16	10	±	7	144	±	14	1093	±	88	72	±	7
NAA measured values	1387	±	29	47,270	±	1384	234	±	7	234	±	7	< LOD			n.m.			1293	±	25	n.m.		
Sarıkamış 1 obsidian (Turkey)																								
inter-laboratory data	325	±	14	5724	±	337	31	±	2	130	±	8	22	±	4	21	±	4	109	±	24	14	±	1
EDXRF measured values	267			6054			29			126			27			22			112			16		
NAA measured values	361			5105			31			133			21			n.m.			81			n.m.		

< LOD: Below minimum limits of detection
n.m.: Not measured

Table 8
EDXRF measurements at MURR of the initial Hatis geological specimens.

Source / specimen	K	Ti	Mn	Fe	Zn	Ga	Rb	Sr	Y	Zr	Nb
Correct source: Hatis obsidian											
AR.2009.48.1	36,665	1418	408	7358	35	17	105	148	7	107	17
AR.2009.72.2	35,004	1495	433	7658	36	16	103	167	8	115	19
AR.2009.72.3	32,889	1179	375	5847	31	13	111	129	6	96	18
AR.2009.73.1	34,501	984	358	5849	32	14	105	116	7	88	18
AR.2009.74.1	34,476	1100	450	6024	33	15	111	114	8	100	21
AR.2009.74.2	36,160	987	377	6281	32	17	111	124	10	100	21
Incorrect source: Gutansar obsidian											
AR.2009.72.1	35,193	1782	474	7525	46	17	146	137	7	177	30
Gutansar means	34,828	1828	524	7642	50	17	144	136	11	180	31
Incorrect source: Mets Arteni obsidian											
AR.2009.75.1	37,206	391	492	4433	35	13	145	7	21	84	37
Mets Arteni means	37,446	414	508	4377	33	14	141	8	25	87	38

4.1. pXRF methods

Based on our preliminary studies, we focused on well-measured elements that best discern the different obsidian types from Hatis. As explained by Hughes (1984:3), it "is not necessarily the case… that the inclusion of larger numbers of variables… results in a 'better' classification" in obsidian artifact sourcing. Poorly measured and uninstructive elements, he states, should be excluded from the dataset and subsequent statistical tests. Shackley (1988:763) agrees, and a "rule of thumb… is to use the fewest variables necessary" (Shackley, 1995:546). Elements that are both well-measured by XRF and highly effective for obsidian sourcing include Rb, Sr, Y, Zr, Nb, and Fe (Frahm, 2014; 2019). Previously published research on Hatis obsidian (Section 2; Table 1) and our own studies (Section 3: Tables 5 to 10) established that we should focus on a set of four elements – Rb, Sr, Zr, and Fe – to discern among the different chemical types of Hatis obsidian using pXRF.

Geological obsidian specimens at Hatis volcano were tested in the field with a Thermo Niton 950 XL3t GOLDD+ instrument (Frahm, 2014; 2016;; Frahm and Feinberg, 2015). This pXRF model is equipped with a silicon drift X-ray detector (SDD) that has an energy resolution $\leq$ 155 eV in practice, and it produces an incident X-ray beam using a miniaturized 2-W tube (Ag anode, 50 kV maximum voltage, and 200 μA maximum current). The instrument has a built-in GPS receiver that can record coordinates with each measurement, and the analyzed spots are displayed live and recorded using a built-in video camera. The elements of interest were measured using the "main" X-ray filter and the corresponding conditions (voltage: 40 kV, current: $\leq$50 μA) for 20 s.

We applied the fundamental parameters (FP) approach to data correction for all analyses in this study. That is, FP was used as a means to account for physical phenomena (e.g., absorption and fluorescence edge energies, incoherent scattering, photoelectric absorption, fluorescent and Coster-Kronig transition yields) that affect the measured X-ray spectra and must be "corrected" during the quantification calculations. Each instrument's factory-set calibration, which was based on a suite of standard reference materials (SRMs) principally certified by the United States' National Institute of Standards and Technology (NIST) and the United States Geological Survey (USGS), was subsequently "fine-tuned" using a collection of 24 obsidian reference standards (Frahm, 2014; this collection was the predecessor of the Peabody–Yale Reference Obsidians, Frahm, 2019). Accuracy of the elements in question was evaluated using three well-characterized obsidian specimens (Table 11): NIST SRM 278 (Newberry Crater, Oregon), USGS RGM-1 (Glass Mountain, California), and MURR GBOR01 (Little Glass Buttes, Oregon). Our values exhibit good agreement with the recommended or certified values for these three obsidians and with the mean values from published datasets.

The field-based use of pXRF instruments allows new approaches for characterizing obsidian sources. For example, Shackley (2005) discusses the cost- and labor-induced restrictions on source sampling and characterization with laboratory-based techniques, resulting in 10–20% of specimens collected across a flow or dome actually being analyzed. Using pXRF in the field reduces the burden placed on probabilistic sampling. Instead, sampling can be shaped less by the logistics of analyzing specimens in a laboratory (e.g., collection and handling, shipping costs) and more by the expression of a source on the landscape. For this study, one priority was localizing the boundaries between the different compositions of obsidian. Coordinates and elevation were recorded for each measurement with the instrument's built-in GPS receiver. Each measurement had at least three replicates, and as many as ten obsidian specimens were analyzed at each locus. Our resulting dataset reflects six days of surveys at Hatis, covering a total of ~60 km by vehicle and ~30 km on foot.

4.2. Results and data analysis

Our pXRF analyses at 80 sampling loci across Hatis volcano revealed four elemental types of obsidian that correspond to discrete areas on the volcanic landscape. As noted in Section 2, various nomenclatures have been applied to obsidian from Hatis (Table 1; e.g., Hatis A and B in Keller et al., 1996; Hatis 1 and 2 in Chataigner and Gratuze, 2014). There is also the potential for confusion with the standard nomenclature for Armenian archaeological sites (e.g., Hatis 1), which are named for the nearest village and numbered in order of discovery. Consequently, we opt to use Greek letters. Two- (Fig. 6) and three-dimensional (Fig. 7) scatterplots based on the elements noted in Section 4.1 – Zr, Rb, Sr, and Fe – reveal four geochemical clusters. The elemental data (means for each of the sampling loci), their GPS coordinates, and the elevations are available in the supplementary materials. Performing discriminant function analysis (DFA) based on the three "mid-Z" trace elements – Zr, Rb, and Sr – yields a function that can account for 99.99% of the dataset variability. The output file from XLSTAT 2019.3.2 is also available in the supplementary materials. Fig. 8 plots the discriminant function for the obsidian types by elevation on the southern slopes, revealing an elevation trend. Each chemical type of obsidian occurs over a range of elevations: alpha at ~1590–1700 m asl, beta at ~1560–1830 m asl, gamma at ~1710–1910 m asl, and delta at ~1960–2100 m asl.

Fig. 9 places the four obsidian types on a topographic map of Hatis. Note that all four occur on the southern slopes of the volcano (Fig. 10), but alpha obsidian is also associated with the perlitic deposits on the northeastern side. It should be stressed, however, that alpha obsidian is manifested differently on the two sides of the volcano. Substantial and prominent obsidian outcrops occur along the southern side of Hatis (Fig. 11a), exposed principally by colluvial forces. These easily accessible and highly visible outcrops yield sizable blocks of nearly flawless obsidian in convenient sizes and forms for knapping. On the northeastern flanks, only small obsidian nodules and lamellae (typically < 2 cm; Fig. 11b), which are associated with much more pumiceous deposits, are exposed only where recent erosion (especially slope failure due to grazing) and human activities (mainly quarrying raw material to make concrete) have cut into the flow. Therefore, the northeastern obsidian not only has low accessibility but also would have served as

Table 9
Comparing the EDXRF and NAA datasets for the initial Hatis specimens using a Student's *t* test.

Technique	K			Mn			Fe			Zn			Rb			Sr			Zr		
Hatis obsidian: high Al-Ti cluster																					
EDXRF	35,834	±	1174	421	±	17	7508	±	212	36	±	1	104	±	1	158	±	13	111	±	5
NAA	32,704	±	3563	500	±	10	7739	±	232	35	±	2	105	±	2	182	±	1	78	±	1
p-value	0.3593			0.0310			0.4080			0.8310			0.5528			0.1243			0.0153		
significant?	no			yes			no			no			no			no			yes		
Hatis obsidian: low Al-Ti cluster																					
EDXRF	34,506	±	1336	390	±	41	6000	±	204	32	±	1	109	±	3	121	±	7	96	±	6
NAA	35,157	±	528	500	±	10	6262	±	60	36	±	1	112	±	1	143	±	1	69	±	2
p-value	0.5613			0.0238			0.1688			0.0028			0.2570			0.0144			0.0032		
significant?	no			yes			no			yes			no			yes			yes		

Table 10
Elemental data for Hatis obsidian types from Martirosyan-Olshansky's research.

reference	*names*	*n*	*Rb*			*Sr*			*Y*			*Zr*			*Nb*			*Fe*		
Martirosyan-Olshansky 2014	Akunq A	5	100	±	4	116	±	7	17	±	1	89	±	2	22	±	1	6006	±	214
	Akunq B	11	88	±	3	203	±	3	17	±	1	113	±	2	20			9135	±	163
Olshansky 2018	Hatis-1	13	111	±	3	101	±	3	19	±	1	97	±	2	23	±	1	6364	±	204
	Hatis-2	16	100	±	4	153	±	17	17	±	1	115	±	6	21	±	1	8835	±	679
	Hatis-3	2	94	±	1	216	±	3	17	±	1	139	±	1	22			11,286	±	78
	Hatis-4	1	97			171			20			119			21			11,695		

Table 11
Assessing accuracy based on well-characterized obsidian specimens.

Source / publication	*Zr*			*Sr*			*Rb*			*Fe*		
NIST SRM 278: Obsidian, Newberry Caldera, Oregon												
This study	272	±	4	70	±	2	123	±	2	13,070	±	290
NIST values (Reed, 1992)				64	±	1	127	±	1	14,280	±	140
Published means (Frahm & Brody, 2019)	292	±	21	65	±	2	128	±	2	14,360	±	660
USGS RGM-1: Obsidian, Glass Mountain, California												
This study	203	±	4	117	±	2	146	±	2	11,710	±	270
USGS values (Smith, 1995)	220	±	20	110	±	10	150	±	8	13,000	±	300
Recommended values (Frahm, 2019)	222	±	4	108	±	2	150	±	3	12,930	±	290
MURR GBOR01: Little Glass Buttes, Oregon												
This study	86	±	3	77	±	3	95	±	4	5940	±	120
MURR values (Glascock & Ferguson, 2012)	96			69			94			6180		
Published means (Frahm & Brody, 2019)	99	±	8	70	±	7	99	±	8	6550	±	610

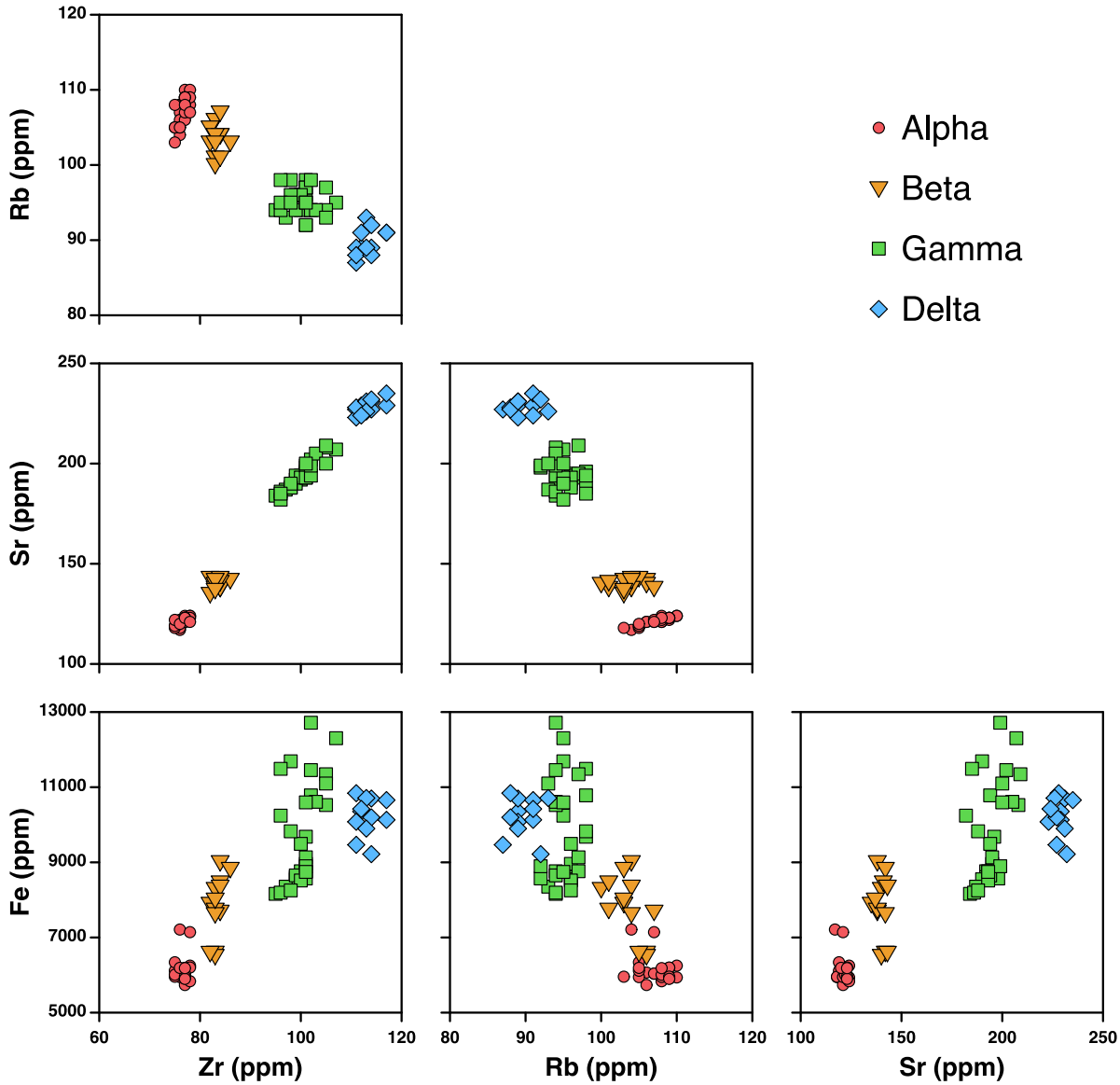

Fig. 6. Matrix of elemental scatterplots for Rb, Sr, Zr, and Fe for the Hatis geological specimens.

poor toolstone due to differences in its emplacement conditions. Therefore, while small quantities of alpha obsidian occur on the northeastern side, the southern slopes have markedly more and better obsidian, and in turn, they were considerably more likely to have served as a location for toolstone acquisition. It must also be noted that outcrops on the southern slopes are so abundant that our loci here are not exhaustive. Instead, our focus in the field was identifying boundaries between chemically different types. Fig. 12 combines the analytical data and our field survey notes with satellite imagery to delineate the obsidian outcrops as well as the approximate distributions of these obsidian types at Hatis volcano.

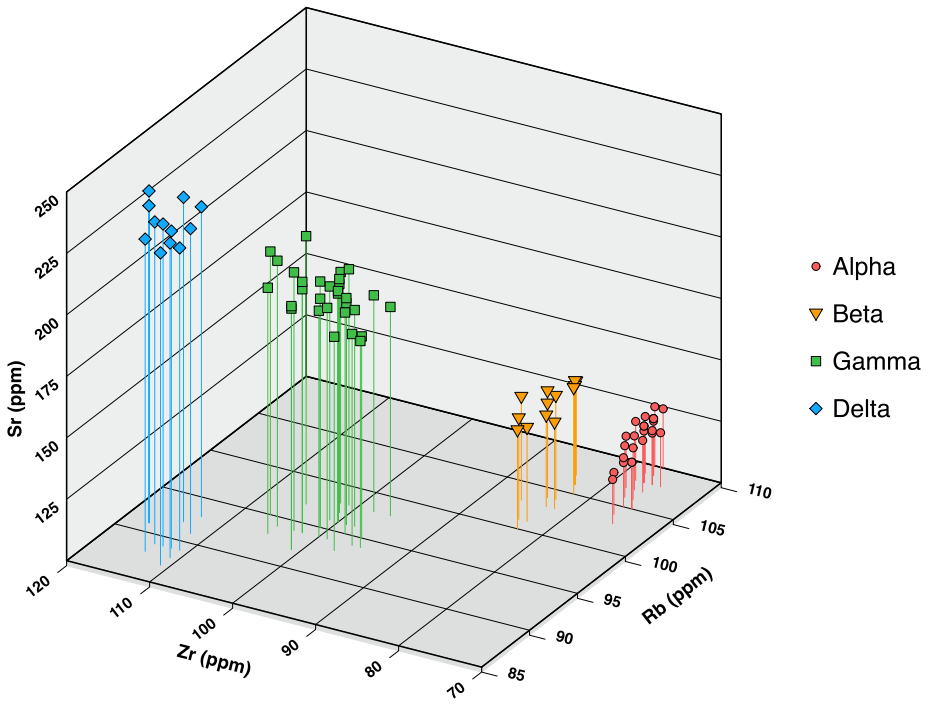

Fig. 7. Three-dimensional elemental scatterplot of Rb, Sr, and Zr for the Hatis geological specimens.

4.3. Geological interpretation

The geological mechanism of these four obsidian types, which fall along a clear geochemical trend, remains uncertain. Given the uncertainties and inconsistencies in dating (Section 2), there is currently no convincing evidence that the four types of obsidian erupted at different times, certainly not hundreds of millennia apart. As shown by the matching elemental data in Table 1, Lebedev et al. (2013) dated the same chemical type of obsidian (i.e., our alpha), despite yielding dates of 740 ± 250 and 480 ± 50 ka, thereby suggesting that their Phases I and II are only a product of the 250-ka error range. Recall that seeking two phases of obsidian-producing volcanism at Hatis dates as far back as Komarov et al. (1972), who simply noted the mismatching ages from FT and ^{40}K–^{40}Ar dating. Hence, it appears to be that seeking two long-separated phases is a wild goose chase.

Despite these unresolved chronological issues, we can propose two basic hypotheses about the formation of these four obsidian types, as simplified and illustrated in Fig. 13. One possibility, as shown in Fig. 13a, is that the four types reflect a series of closely timed eruptions and/or intrusions between which the magma slightly changed, yielding four overall similar but still somewhat distinct lavas stacked atop one other. A second possibility, as shown in Fig. 13b, is that the magma chamber was chemically zoned such that, during one voluminous eruption, the lava changed in composition as it erupted. Under such a scenario, during emplacement, the zoned and highly viscous lava folded over onto itself, yielding four discrete geochemical steps, rather than continuous variation, exposed at the surface. That is, the lava could have exhibited continuous chemical variation as it erupted, but only small segments of that variation remain accessible at or near the surface.

There are examples of both hypothesized models elsewhere, although the best-documented cases come from the American Pacific Northwest. As noted in the Introduction, this region is not an ideal analog for volcanism within the Armenian Highlands; however, Dixon (1976) noted that some parts of the Pacific Northwest are roughly analogous to this region. The analog for the first scenario (Fig. 13a) comes from Newberry National Volcanic Monument in Oregon (Fig. 14). The caldera of Newberry Volcano (~7–8 km in diameter) contains several Holocene obsidian-bearing lava flows, including (as shown in Fig. 14b) Big Obsidian Flow, East Lake Obsidian Flows, Buried Obsidian Flow, and Game Hut Obsidian Flow. Obsidian specimens from these four flows were measured using NAA (Ambroz, 1997), and Fig. 14a is a scatterplot of the Rb vs. Mn measurements, establishing that these obsidian flows are chemically similar but still distinct. Ambroz's (1997) use of NAA restricts those elements in common with our pXRF measurements, but comparing Fig. 14a for Newberry and Fig. 6 for Hatis yields tantalizing similarities. Big Obsidian Flow is the best dated based, in large part, on radiocarbon dating of a tree caught up in the eruption (USGS 755: 1340 ± 60 uncalibrated BP). After calibration, the eruption occurred ~1200–1300 years ago. The other flows are not as well dated. Obsidian hydration offers some constraints (Friedman, 1977) and yield rough ages of ~3500 years for the East Lake Obsidian Flows and ~6700 years for the Game Hut Flow. Consequently, this entire eruptive sequence might have occurred in five millennia. One key challenge of testing this model at Hatis volcano is clear: the error ranges for the ^{40}Ar–^{39}Ar ages (e.g., 480 ± 50 ka, Lebedev et al., 2013) are greater than the potential eruption intervals in such a scenario.

An analog for the second scenario (Fig. 13b) comes from the Borax Lake rhyolitic lava dome in northern California (Fig. 15). Bowman et al. (1972), Bowman et al. (1973a), Bowman et al. (1973b) recognized that obsidian from the Borax Lake dome exhibited a continuous range of compositions, as demonstrated in Fig. 15a. The likeliest mechanism, they propose, is mixing of two magmas with distinct compositions in different proportions. Nevertheless, obsidian sourcing was still possible because the chemical pattern "is just as definitive as it would be if the flow were extremely homogeneous" (Bowman et al., 1973b: 123). USGS geologists mapped the Borax Lake dome as a single rhyolitic eruption circa 91 ± 13 ka (facies "rb" in Fig. 15b–c), but Hearn et al. (1995) note the potential for mixing with a dacite (facies "dcpk") and/or basaltic andesite ("bar"). Hence, the Borax Lake dome appears to be a rare example of clear chemical variation within a single obsidian source, but studies are complicated by the construction of a neighborhood directly atop this dome. Although artifacts have been attributed to the Borax Lake source (e.g., Ericson and Berger, 1974), a lack of published data means that it is difficult to predict what effect human exploitation might have on observable elemental patterns in artifacts, not just geological specimens. For example, Jackson (1989:87) notes the variable qualities of Borax Lake obsidian (i.e., "… from pumiceous material to a relatively

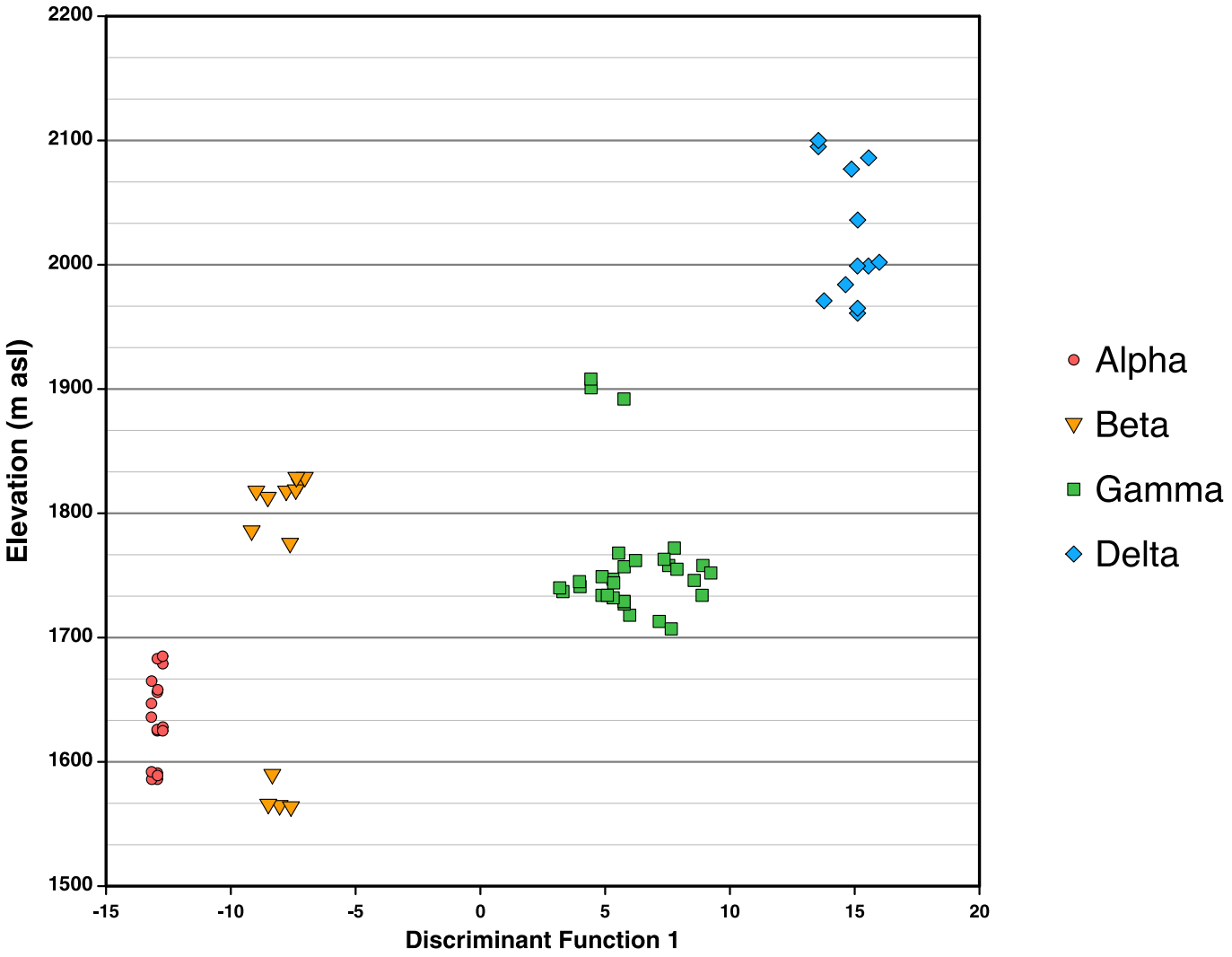

Fig. 8. Scatterplot of a discriminant function (based on Rb, Sr, and Zr) vs. outcrop elevation, showing the differences in the obsidian chemical types with height on the volcano.

dense glass" that "ranges from a dark gray-black to a gray 'frothy' appearance"). It remains unclear if past knappers' selection of the best toolstone could yield a narrower range of chemical compositions than reported in specimens tested at Lawrence Berkeley National Laboratory (Bowman et al., 1972, 1973a, 1973b).

Distinguishing between these two scenarios represents a considerable challenge for future research. The published dating uncertainties, at present, are 40 to 50 thousand years; however, the timing between separate eruptions could be a few millennia (or even shorter). In addition, research drilling, such as the 150-m-deep core taken from Obsidian Dome in eastern California (Eichelberger et al., 1984), might be necessary to better understand the internal structure of Hatis. Ultimately, for now, the timing and relationships of these Hatis obsidian flows are open issues due, in large part, to the rarity of the above examples, meaning characteristic trends remain elusive.

5. Archaeological example: NG1

The site of NG1 lies just 12 km from Hatis volcano, and its lithic assemblage consists entirely of obsidian from numerous volcanoes across the Armenian Highlands. Between 2012 and 2017, we analyzed 2351 obsidian artifacts from NG1 using pXRF (this number was only 316 as of Adler et al., 2014). Of these, 40 artifacts (1.70%) originated from the obsidian flows of Hatis.

5.1. NG1: The site and its excavations

The open-air site of NG1 (40.34679° N, 44.59706° E, 1400 m asl) over a length of ~135 m in the western wall of a gorge cut by the Hrazdan River (Fig. 16). Attempted road construction exposed a section of fine- and coarse-grained fluvial sediments and paleosols, forming in both floodplain and channel environments. Obsidian artifacts were found throughout the sequence. They are likely in situ in the floodplain deposits and palaeosols but reworked in the channel sands and gravels (Adler et al., 2014; Sherriff et al., 2019). The fluvial sediments are bounded above ("Lava 1" of Adler et al. 2014, "HGW-VI" of Sherriff et al., 2019) and below ("Lava 7", "HGW-IV") by lava flows emanating from the Gegham range (Adler et al., 2014; Sherriff et al., 2019), and were deposited in floodplain and channel environments (Sherriff et al., 2019). Lava 1 and Lava 7 flows have been $^{40}Ar/^{39}Ar$ dated to 197 ± 7 and 441 ± 6 ka, respectively (Adler et al., 2014), while sanidine grains among volcanic tephra in the top fine-grained alluvial unit were also dated by $^{40}Ar/^{39}Ar$ to 308 ± 3 ka, revealing a stratigraphic unconformity between the sedimentary sequence and the capping lava. Thus, artifacts contained in these sediments date between ~310 and ~440 ka, representing behaviors between MIS 11 (~424–374 ka) and 9 (~337–300 ka). After its discovery in 2008, NG1 was excavated by the Hrazdan Gorge Palaeolithic Project until 2017 (Adler et al., 2012, 2014). Excavations from 2008 to 2013 focused on the northern portion of the

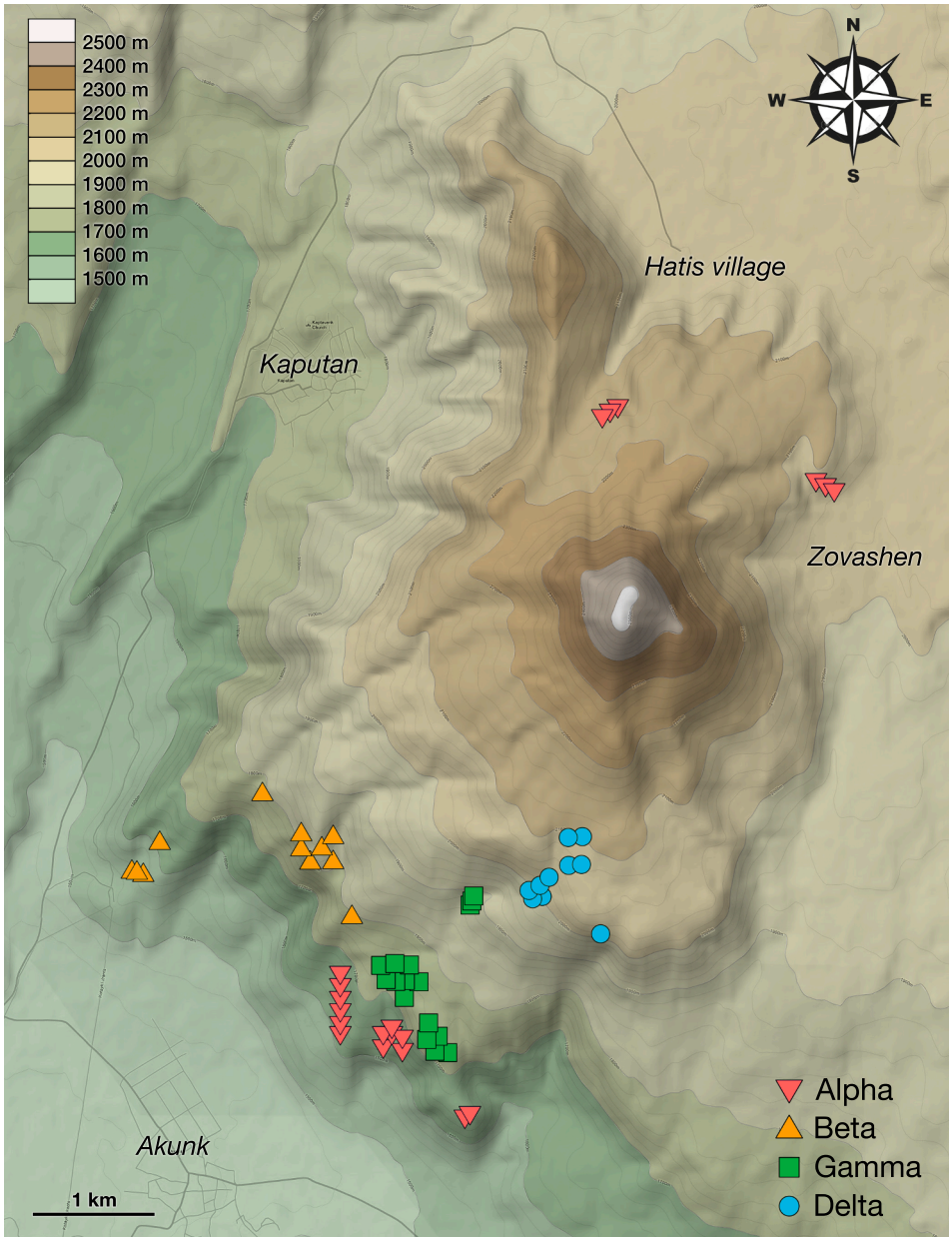

Fig. 9. A topographic map of Hatis volcano illustrates the locations and elevations of our 80 sampling loci and the corresponding obsidian type at each one. Village names are italicized.

site, where artifacts attributed to MIS 9e (~335–325 ka) exhibit the earliest evidence of the Mode 2 to 3 (i.e., Acheulian to Levallois) technological transition (Adler et al., 2014). In particular, the same stratigraphic layer contains Levallois cores and flakes as well as Acheulian bifaces, including some reused as hierarchical cores. Archaeological and geochronological work is ongoing for the site's southern portion, which was excavated from 2015 to 2017; however, it can be reported that the lithic artifacts from this part of the site reflect bifacial technology without hierarchical core reduction techniques. Both NG1 and the Pleistocene stratigraphy of the Hrazdan River valley have previously been discussed in the literature (see Adler et al., 2014; Sherriff et al., 2019, respectively), to which readers are referred for greater detail.

5.2. pXRF methods

The artifacts from NG1 were analyzed in Armenia between in 2012 and 2017, and thus, the instrument model changed as pXRF technology advanced. In 2012, we analyzed obsidian artifacts in the Hrazdan Gorge Palaeolithic Project's field laboratory in Yerevan using a Thermo Niton XL2 500 pXRF instrument. This model had a Si P-N diode detector with a resolution $\leq$ 180 eV in practice, and it produced X-rays using a 2-W tube (Ag anode, 45 kV maximum voltage, 80 μA maximum current). The elements of interest were measured using the "main" filter and its corresponding analytical conditions (voltage: 45 kV, current: $\leq$44 μA) for 40–80 s. Between 2014 and 2017, artifacts from NG1 were analyzed in Armenia using the same Niton 950 XL3t GOLDD+ instrument described in Section 4.1. In addition, these instruments used FP correction and the same set of obsidian specimens for calibration.

5.3. Sourcing results

Appling the DFA from Fig. 8 to the 40 NG1 artifacts results in their attribution to the alpha, beta, gamma, and delta types of Hatis obsidian. In Fig. 17, the NG1 artifacts are plotted individually, whereas a box-

Fig. 10. Outcrops of (a) gamma-type obsidian and (b) alpha-type obsidian at Hatis volcano.

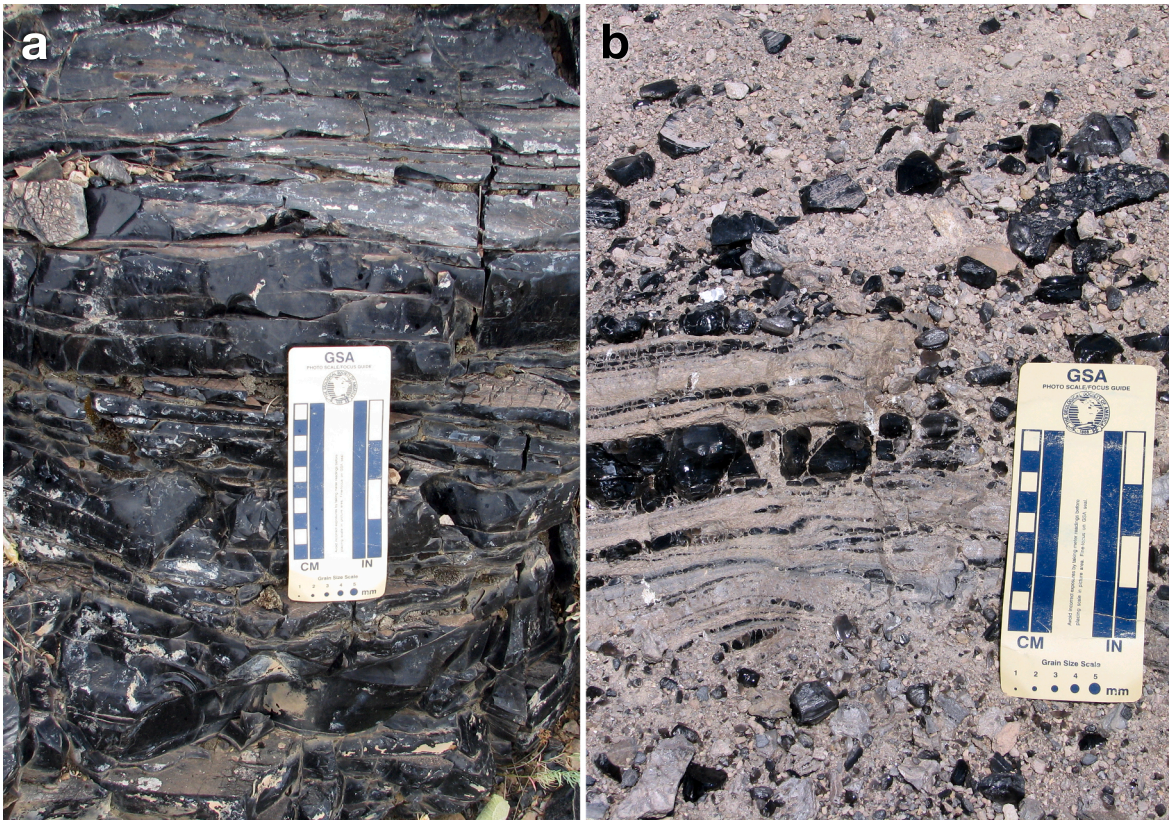

Fig. 11. Large outcrops of alpha obsidian (a) occur on the southern slopes of Hatis volcano, while (b) the northeastern flanks have only small nodules and lamellae of largely perlitic obsidian.

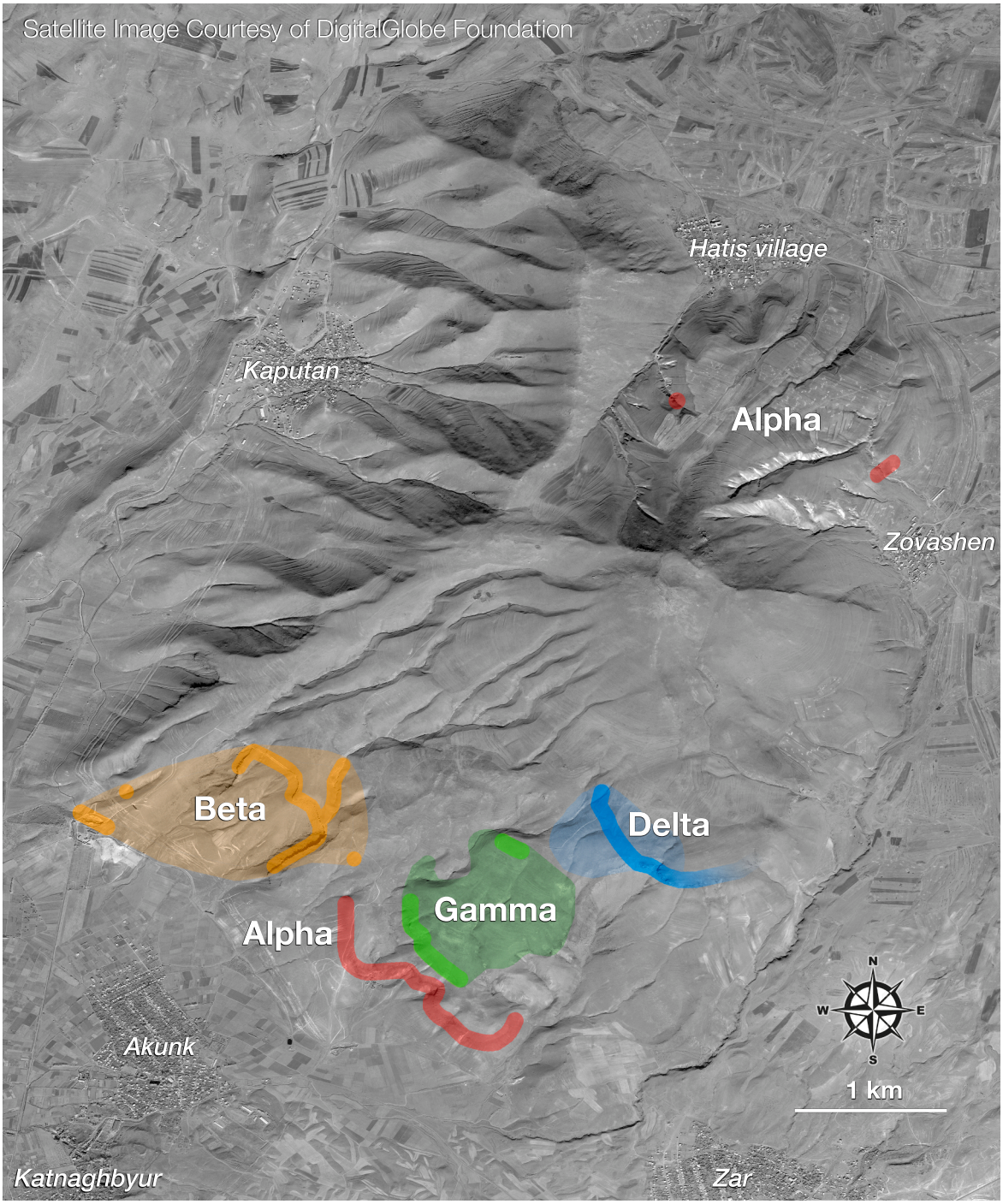

Fig. 12. A satellite image of Hatis volcano, when combined with our analytical data and field notes, delineates the approximate distributions of the four obsidian types on the landscape. Satellite image courtesy of DigitalGlobe Foundation.

percentile plot (Esty and Banfield, 2003) illustrates the distribution of the elemental data for the geological specimens. This plot establishes that each of the four Hatis obsidian types is present among the sourced NG1 assemblage, despite the fact that the outcrops span more than 500 m in elevation on the volcanic slopes.

5.4. Archaeological interpretation

Artifacts of gamma- and delta-type obsidian occur in the NG1 assemblage but are scarce. Today, exposures of alpha and beta obsidian are highly visible as one passes by the volcano, especially on a sunny day, when sunlight glistens off of the glassy fragments. Due to less tectonic uplift, though, it is possible that such visibility was less pronounced when NG1 was occupied. Erosion is another force to consider. Within the confines of our proposed models (Fig. 13a-b), outcrops of the different obsidian types might have shifted, to some extent, not only in precise location but also the degree of exposure. Likely erosive processes at Hatis would include volcanic and fluvial activity, freeze–thaw weathering, and Quaternary climatic changes subsequent to the obsidian emplacement. Such forces certainly altered those spots on the volcanic slopes where obsidian could be collected, although they could not transpose the lower- and higher-elevation outcrops. Today the surroundings are mountain

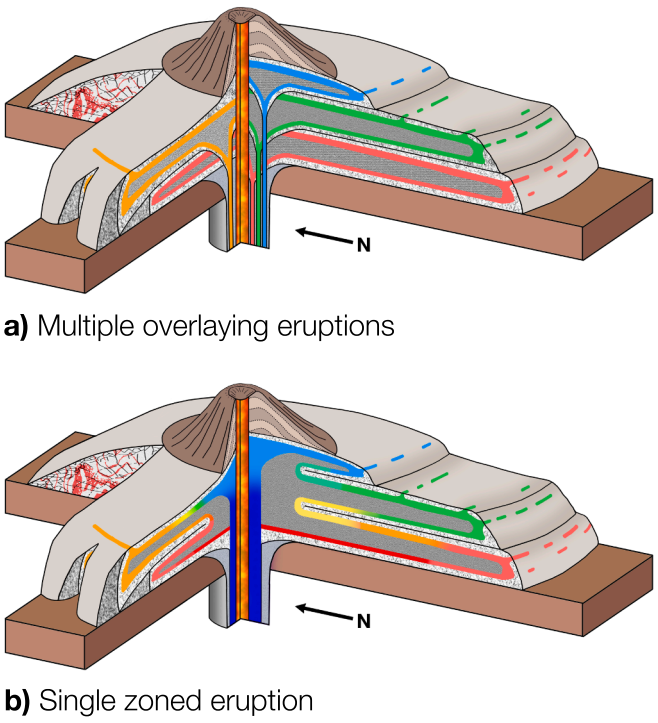

Fig. 13. Simplified cross-sections of Hatis volcano to illustrate the two potential mechanisms for our observed shifts in obsidian composition: (a) the four types reflect a series of closely timed eruptions, yielding four similar but still distinct lavas stacked atop one other, or (b) the magma chamber was chemically zoned such that the lava changed in composition as it erupted but folded over onto itself, yielding four discrete geochemical steps rather than continuous variation at the surface.

steppe, and there is currently no tree cover at Hatis, albeit paleoenvironmental data are lacking to establish how far we can extrapolate from the current ecological conditions back into the Pleistocene, even during interglacials when NG1 was occupied. Certainly, tree cover might affect the visibility and accessibility of the different outcrops. In recent times, Hatis volcano has been covered by ~50 cm of snow between December and April (Badalyan et al., 2004), so access to obsidian outcrops is limited seasonally, and we assume that this would have been the case in the past as well.

Today one must bypass the lower outcrops of alpha and beta obsidian and climb higher to encounter the gamma and delta obsidian outcrops, and this would, in general, have been true in the past. Despite visiting Hatis volcano multiple times, starting in 2011, we did not find the high delta-type outcrops until 2016. We can attest that bypassing the alpha and beta outcrops to obtain gamma and delta obsidian requires more energy, the expenditure of which makes little sense given that there are no discernable differences in the flaking quality (or "knappability") among the four types. This suggests that collection from the higher-elevation outcrops might indicate embedded procurement, which would be consistent with acquisition of Gutansar obsidian at NG1 reported by Frahm et al. (2019). Utilizing the higher-elevation types makes the most sense in the context of other activities, such as logistical subsistence forays and/or wayfinding/reconnaissance (i.e., gaining a higher view of the distribution of resources and other groups on the landscape below).

Nevertheless, caution regarding such an interpretation is still warranted. To date, no rivers are known to have transported Hatis obsidian any great distance from its slopes, and the obsidian is not known in secondary deposits on the plains surrounding this volcano (Badalyan et al., 2004). The authors' surveys of the Hrazdan basin, which included identification and pXRF analysis of obsidian pebbles in alluvial and floodplain deposits (Frahm et al., 2016, 2017), did not identify any deposits of Hatis-derived obsidian. It must be recognized, however, that much of this survey work focused on times that predate the emplacement of Hatis obsidian, which undermines its direct relevance to this

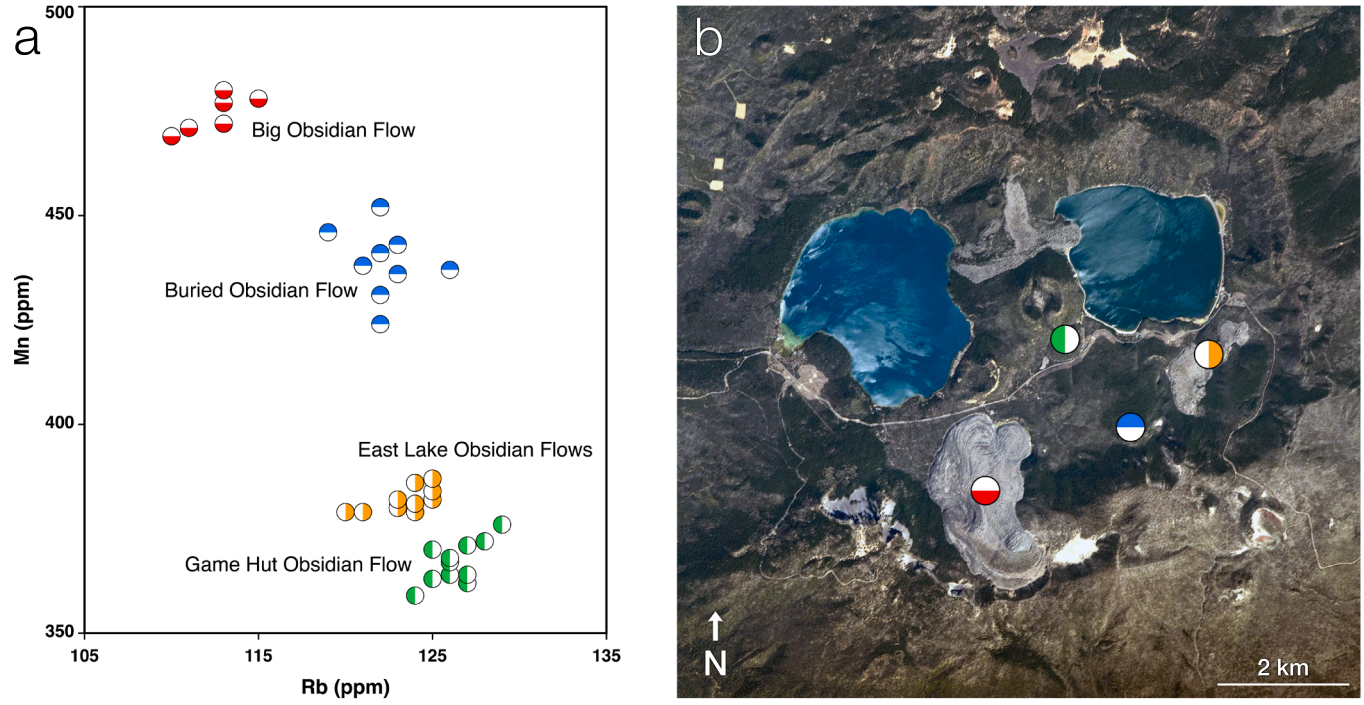

Fig. 14. (a) A scatterplot of elemental data (Rb vs. Mn measured by NAA) for four different obsidian flows at Newberry volcano, extracted from Ambroz (1997) using WebPlotDigitizer v4.4, and (b) the corresponding locations of these flows inside the volcanic caldera. The image is a cropped version of astronaut photograph #ISS063-E-70532, which was acquired on August 13, 2020, and it is provided by the ISS Crew Earth Observations Facility and the Earth Science and Remote Sensing Unit, Johnson Space Center, which freely shares space photography for use by the public.

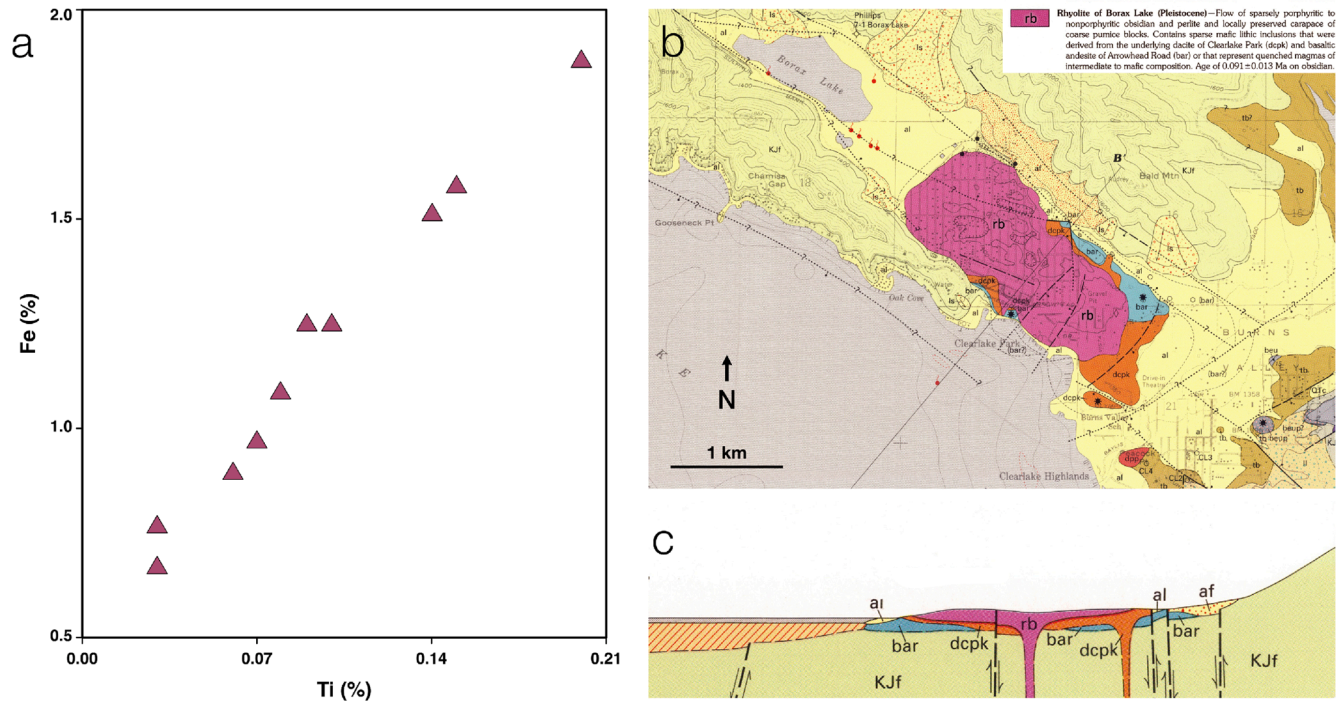

Fig. 15. (a) A scatterplot of elemental data (Ti vs. Fe measured by NAA) for obsidian from the Borax Lake dome, as reported by Bowman et al. (1973b) as well as (b) a plan and (c) cross-section view of the dome (the pink feature labeled "rb") as mapped by USGS geologists (Hearn et al., 1995).

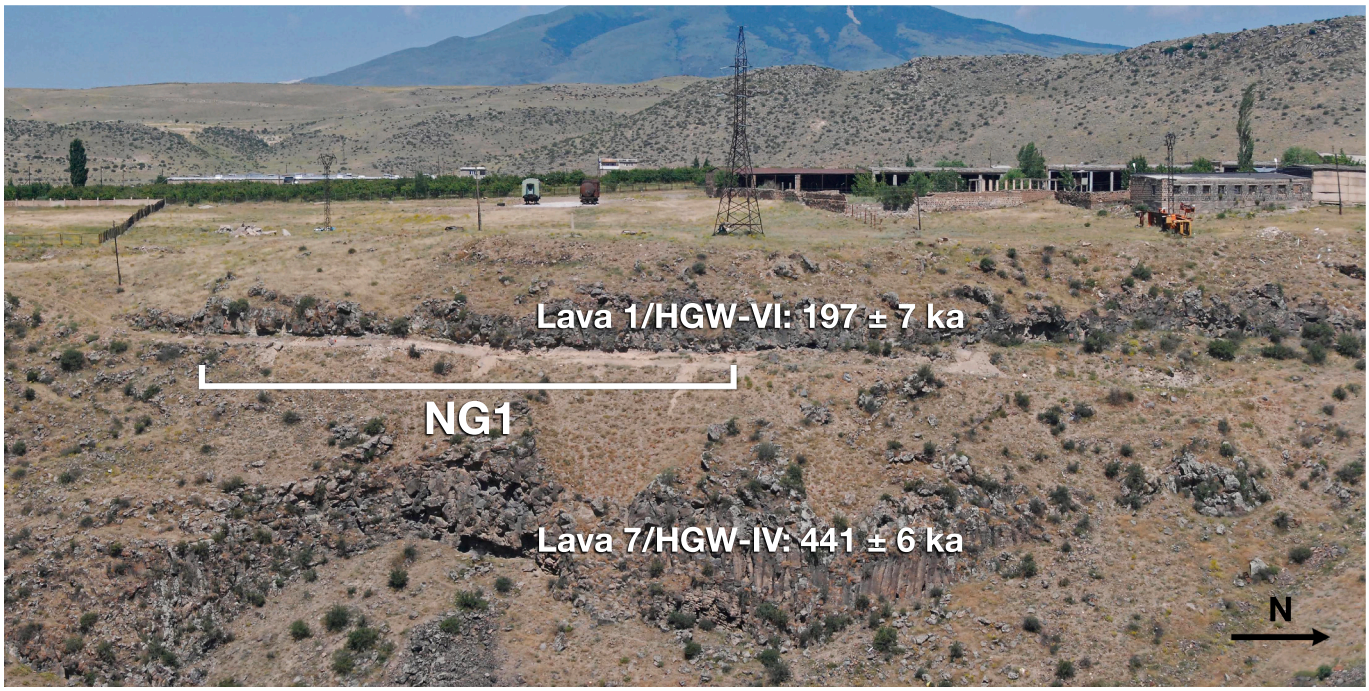

Fig. 16. Photograph of NG1, looking toward the west from the eastern side of the Hrazdan valley, and the associated volcanic features, specifically the two dated lava flows.

issue (Sherriff et al., 2019). At present, we do not have strong reasons to hypothesize that the NG1 occupants were able to collect Hatis obsidian from secondary deposits a notable distance from the slopes of the volcano. We must, though, entertain the possibility the delta-type artifact is a result of erosion and gravity (i.e., a delta-type block tumbled to a lower elevation).

6. Discussion

It remains uncertain how much of a geological oddity Hatis volcano is and how much of its unusual character is due to its occurrence in the milieu of the Armenian Highlands instead of, say, the American Pacific Northwest. The complex tectonics and subduction of the region are topics of active research (e.g., Avagyan et al., 2018; Hässig et al., 2019;

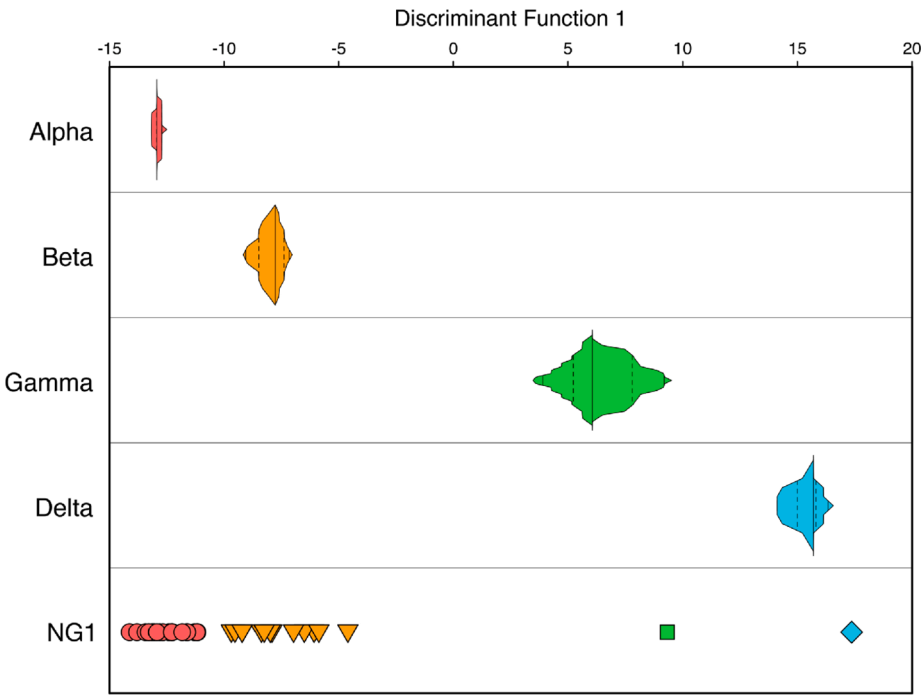

Fig. 17. A discriminant function (based on Rb, Sr, and Zr) separates the Hatis obsidian types in (top) the geological specimens using a box-percentile plot (Esty and Banfield, 2003) and (bottom) the NG1 artifacts, which are plotted individually. Greater spread among the artifacts is, we suggest, primarily due to analyzing weathered, irregular artifact surfaces rather than fresher, flatter outcrop surfaces. In this plot, the shape width at any point is proportional to the percentile. The median value is marked by a solid line at the widest point, the first and third quartiles are denoted by dashed lines, the 5th and 95th percentiles are marked by solid lines, and the points on each side are the maxima and minima for that particular obsidian type.

Halama et al., 2020; Lin et al., 2020; Sugden et al., 2020). As implied by Shirinian and Karapetian (1964), it may well be that models of obsidian-producing rhyolitic volcanism are based too much on observations from the relatively geologically straightforward cases of plate subduction along the so-called Pacific Ring of Fire. That is, common descriptions of obsidian-bearing lava flows and domes (e.g., Fink, 1987; Hughes and Smith, 1993; Shackley, 2005) may well be most relevant in the North American West but less applicable to other geological settings, such as the divergent plate boundary of the East African Rift System or rhyolitic volcanism in the middle of a continental or an oceanic tectonic plate. On the other hand, it might be such complexity of obsidian sources is more common than is generally appreciated. Cobean (2012) compared the chemical characterization of obsidian sources, at least in many parts of the world, to the Apollo moon missions: after visits during the 1960s and 1970s to grab a few specimens of rock, scientists never returned. Given how few specimens have often been used to define their elemental "fingerprints," such complexity of obsidian sources might be more common.

For reasons that are not yet clear, Hatis volcano has a deceptively simple appearance for an obsidian source. Connecting obsidian composition to a location (or locations) in space is, of course, the goal of obsidian sourcing (Neff, 1998), and one challenge of attributing an artifact to a specific source is, as discussed by Green (1998:227), "characterizing the size of the dot which pinpoints its supposed origin." As a result of the research that we document here, it is possible to more precisely define the origins of obsidian artifacts that derived from Hatis. It should be highlighted that this was an iterative process. We did not follow Cobean's (2012) "Apollo moon mission" model. In particular, we did not simply drive to the volcanic outcrops, take a handful of obsidian specimens, send them to a distant analytical laboratory, and never return. Instead, we propose that sampling and surveying, on one hand, and conducting chemical analyses, on the other, are best when integrated and cyclical or repeated, permitting a more nuanced understanding of an obsidian source. It is not a coincidence that the four chemical types of obsidian from Hatis volcano were identified using pXRF, an analytical technique that allowed us to integrate our field and (traditionally) "lab" work.

7. Conclusions

Four compositional types of obsidian occur at Hatis volcano and fall into a clear geochemical trend as elevation increases, but the precise geological mechanism for these different types remains unclear. Fortunately, from an archaeological perspective, it is not essential to understand the exact eruptive mechanisms to use the obsidian types' different elevation ranges as an investigative tool. Our ability to recognize and map these types was predicated on our use of pXRF in the field instead of random transects or probabilistic sampling. This technique also permitted us to not only analyze 2351 obsidian artifacts from the Lower Palaeolithic site of NG1 but also recognize 40 Hatis-derived artifacts from the site, reflecting all four obsidian chemical types. Given that the outcrops of these chemically distinct types span more than 500 m (from $<$ 1600 to greater than 2100 m asl) in elevation on the volcanic slopes, sourcing obsidian artifacts that derive from Hatis volcano enables future studies on links between altitude and behaviors linked to hominin toolstone acquisition.

Declaration of Competing Interest

The authors declare that they have no known competing financial interests or personal relationships that could have appeared to influence the work reported in this paper.

Acknowledgements

This work is dedicated to our friend Sergey Karapetyan, who passed away before we could share our findings with him. His research at Hatis volcano is one foundation on which we built this study, and it was always a pleasure to climb around volcanoes with him. We thank Pavel Avetisyan, Director of the Institute for Archaeology and Ethnography, National Academy of Sciences, Republic of Armenia, for his continued support of our research, and we also thank Khachatur Meliksetyan, Director for Geological Science, National Academy of Sciences, Republic of Armenia for his support and collaboration. Frahm's work was supported, in part, by the University of Sheffield's Department of Archaeology; the NARNIA Project, funded by the European Union and FP7 (Grant #265010); and the Earth Sciences Department, Institute for

Rock Magnetism, Global Programs and Strategy Alliance, and Anthropology Department at the University of Minnesota. Financial support for the Hrazdan Gorge Palaeolithic Project was provided to Adler by the Norian Armenian Programs Committee (University of Connecticut, 2008–2015), two Large Faculty Grants (University of Connecticut, 2008 and 2012), and the L.S.B. Leakey Foundation (2010 and 2011). The PAGES Project, directed by Wilkinson, was funded by the Leverhulme Trust (RPG-2016-102). Other field and/or research assistance was provided by (in alphabetical order): Dmitri Arakelyan, Hayk Azizbekyan, Emily Beverly, Simon Blockley, Alex Brittingham, Jayson Gill, Hayk Haydosyan, Andrew Kandel, Suren Kesejyan, Monika Knul, Masha Krakovsky, Ariel Malinsky-Buller, Christina Manning, Hovik Partevyan, Artur Petrosyan, Katie Preece, Beverly Schmidt-Magee, Rhys Timms, and Benik Yeritsyan.

Appendix A. Supplementary data

Supplementary data to this article can be found online at https://doi.org/10.1016/j.jasrep.2021.103097.

References

Adler, D.S., Yeritsyan, B., Wilkinson, K.N., Pinhasi, R., Bar-Oz, G., Nahapetyan, S., Bailey, R., Schmidt, B.A., Glauberman, P., Wales, N., Gasparian, B., 2012. The Hrazdan Gorge Palaeolithic Project, 2008–2009. In: Avetisyan, P., Bobokhyan, A. (Eds.), Archaeology of Armenia in Regional Context, Proceedings of the International Conference Dedicated to the 50th Anniversary of the Institute of Archaeology and Ethnography Held on September 15-17, 2009 in Yerevan, Armenia. NAS RA Gitutyn Publishing house, Yerevan, pp. 21–37.

Adler, D.S., Wilkinson, K.N., Blockley, S., Mark, D., Pinhasi, R., Schmidt-Magee, B.A., Nahapetyan, S., Mallol, C., Berna, F., Glauberman, P.J., Raczynski-Henk, Y., Wales, N., Frahm, E., Jöris, O., MacLeod, A., Smith, V., Cullen, V., Gasparyan, B., 2014. Early Levallois technology and the transition from the Lower to Middle Palaeolithic in the Southern Caucasus. Science 345 (6204), 1609–1613.

Ambroz, J.A., 1997. Characterization of Archaeologically Significant Obsidian Sources in Oregon by Neutron Activation Analysis. Master's Thesis. University of Missouri-Columbia.

Arutyunyan, E.V., Lebedev, A.V., Chernyshev, I.V., Sagatelyan, A.K., 2007. Geochronology of Neogene-Quaternary volcanism of the Geghama highland (Lesser Caucasus, Armenia). Dokl. Earth Sci. 416, 1042–1046.

Avagyan, A., Sosson, M., Sahakyan, L., Sheremet, Y., Vardanyan, S., Martirosyan, M., Muller, C., 2018. Tectonic evolution of the Northern margin of the Cenozoic Ararat basin, Lesser Caucasus, Armenia. J. Petrol. Geol. 41 (4), 495–511.

Badalyan, R., Chataigner, C., Kohl, P., 2004. Trans-Caucasian obsidian: The exploitation of the sources and their distribution. In: Sagona, A. (Ed.), A View from the Highlands: Archaeological Studies in Honour of Charles Burney. Peeters, Lueven, pp. 437–465.

Bader, N., Merpert, N.J., Muchae, R.M., 1994. Les Importations d'Obsidienne sur les Sites des IXe-VIIe Millénaires B.P. du Djebel Sinjar. Paléorient 20 (2), 6–8.

Blackman, M., 1984. Provenance studies of Middle Eastern obsidian from sites in Highland Iran. In: Lambert, J.B. (Ed.), Archaeological Chemistry III, pp. 19-50.

Blackman, M.J., Badalian, R., Kikodze, Z., Kohl, P.L. 1998. Chemical characterization of Caucasian obsidian geological sources. In: Cauvin, M.-C., Gourgaud, A., Gratuze, B., Arnaud, N., Poupeau, G., Poidevin, J.L., Chataigner, C. (eds.), L'obsidienne au Proche et Moyen-Orient: Du Volcan à l'Outil. BAR International Seriespp. 205–231.

Bowman, H., Asaro, F., Pearlman, I. 1972. On the University of Composition in Obsidians and Evidence for Magma Mixing. University of California, Lawrence Berkeley Lab Report LBL-661.

Bowman, H.R., Asaro, F., Perlman, I., 1973a. Composition variations in obsidian sources and the archaeological implications. Archaeometry 15 (1), 123–127.

Bowman, H.R., Asaro, F., Perlman, I., 1973b. On the Uniformity of Composition in Obsidians and Evidence for Magmatic Mixing. J. Geol. 81 (3), 312–327.

Carballo, D.M., Carballo, J., Neff, H., 2007. Formative and classic period obsidian procurement in Central Mexico: a compositional study using laser ablation–inductively coupled plasma–mass spectrometry. Lat. Am. Antiq. 18 (1), 27–43.

Chataigner, C., Gratuze, B., 2014. New data on the exploitation of obsidian in the southern Caucasus (Armenia, Georgia) and Eastern Turkey, part 1: source characterization. Archaeometry 56 (1), 25–47.

Chataigner, C., Badalian, R., Bigazzi, G., Cauvin, M.-C., Jrbashian, R., Karapetian, S.G., Norelli, P., Oddone, M., Poidevin, J.-L., 2003. Provenance Studies of Obsidian Artefacts from Armenian Archaeological Sites Using the Fission-Track Dating Method. J. Non-Cryst. Solids 323 (1-3), 167–171.

Cherry, J.F., Faro, E.Z., Minc, L., 2010. Field survey and geochemical characterization of the southern Armenian obsidian sources. J. Field Archaeol. 35 (2), 147–163.

Cobean, R., 2012. Discussant for "A World of Obsidian: Sourcing, Dating, and Beyond. Annual Meeting of the Society for American Archaeology, Memphis, 18-22 April.

de B. Pereira, C.E., Miekeley, N., Poupeau, G., Küchler, I.L., 2001. Determination of minor and trace elements in obsidian rock samples and archaeological artifacts by laser ablation inductively coupled plasma mass spectrometry using synthetic obsidian standards. Spectrochim. Acta B At. Spectrosc. 56 (10), 1927–1940.

Dixon, J., 1976. Obsidian Characterization Studies in the Mediterranean and Near East. In: Taylor, R.E. (Ed.), Advances in Obsidian Glass Studies: Archaeological and Geochemical Perspectives. Noyes Press, Park Ridge, New Jersey.

Dixon, J.E., Cann, J.R., Renfrew, C., 1968. Obsidian and the Origins of Trade. Sci. Am. 218 (3), 38–46.

Eichelberger, J.C., Lysne, P.C., Younker, L.W., 1984. Research drilling at Inyo Domes, Long Valley Caldera, California. EOS, Trans., Am. Geophys. Union 65 (721), 723–725.

Eichelberger, J.C., Carrigan, C.R., Westrich, H.R., Price, R.H., 1986. Nonexplosive silicic volcanism. Nature 323, 598–602.

Ericson, J.E., Berger, R., 1974. Late Pleistocene American obsidian tools. Nature 249 (5460), 824–825.

Esty, W., Banfield, J.D., 2003. The box-percentile plot. J. Stat. Softw. 8 (17), 1–14.

Fink, J.H., 1980. Surface folding and viscosity of rhyolite flows. Geology 8, 250–254.

Fink, J.H., 1987. The Emplacement of Silicic Domes and Lava Flows. Geological Society of America, Special Paper, p. 212.

Fink, J.H., 1994. Volcanoes: A planetary perspective. Science 263 (5145), 402–404.

Fink, J.H., Manley, C.R., 1987. Origin of pumiceous and glassy textures in rhyolite flows and domes. The emplacement of silicic domes and lava flows. Geol. Soc. Am. Spec. Paper 212, 77–88.

Frahm, E., 2010. The Bronze-Age obsidian industry at Tell Mozan (ancient Urkesh), Syria. Ph.D. dissertation, Department of Anthropology. University of Minnesota-Twin Cities.

Frahm, E., 2012. Non-destructive sourcing of Bronze-Age Near Eastern obsidian artefacts: redeveloping and reassessing electron microprobe analysis for obsidian sourcing. Archaeometry 54 (4), 623–642.

Frahm, E., 2014. Characterizing obsidian sources with portable XRF: Accuracy, reproducibility, and field relationships in a case study from Armenia. J. Archaeol. Sci. 49, 105–125.

Frahm, E., 2016. Can I get chips with that? Obsidian sourcing down to the microdebitage with portable XRF. J. Archaeolog. Sci.: Rep. 9, 448–467.

Frahm, E., 2019. Introducing the Peabody-Yale Reference Obsidians (PYRO) sets: Open-source calibration and evaluation standards for quantitative X-ray fluorescence analysis. J. Archaeolog. Sci.: Rep. 27, 101957.

Frahm, E., Brody, L.R., 2019. Origins of obsidian at the "Pompeii of the Syrian Desert:" Sourcing lithic artifacts from the Yale-French excavations at Dura-Europos. J. Archaeolog. Sci.: Rep. 24, 608–622.

Frahm, E., Feinberg, J.M., 2015. Reassessing obsidian field relationships at Glass Buttes, Oregon. J. Archaeolog. Sci.: Rep. 2, 654–665.

Frahm, E., Feinberg, J.M., Schmidt-Magee, B.A., Wilkinson, K.N., Gasparyan, B., Yeritsyan, B., Adler, D.S., 2016. Middle Palaeolithic toolstone procurement behaviors at Lusakert cave 1, Hrazdan valley. Armenia. J. Hum. Evol. 91, 73–92.

Frahm, E., Sherriff, J., Wilkinson, K.N., Beverly, E.J., Adler, D.S., Gasparyan, B., 2017. Ptghni: A new obsidian source in the Hrazdan River Basin, Armenia. J. Archaeolog. Sci.: Rep. 14, 55–64.

Francaviglia, V., Palmieri, A.M., 1998. Analisi di Ossidiane dell'Area del Habur (Giazira Settentrionale). In: Pecorella, P.E. (Ed.), Tell Barri/Kahat 2: Relazione Sulle Campagne 1980–1993 a Tell Barri/Kahat, nel Bacino del Habur (Siria). CNR, Rome, pp. 335–344.

Friedman, I., 1977. Hydration Dating of Volcanism at Newberry Volcano, Oregon. Journal of Research of the U.S. Geological Survey 5, 337–342.

Gasparyan, B., Arimura, M., 2014. Study of the Stone Age in the Republic of Armenia: Achievements and perspectives. In: Gasparyan, B., Arimura, M. (Eds.), Stone Age of Armenia: A Guide-Book to the Stone Age Archaeology in the Republic of Armenia. Center for Cultural Resource Studies, Kanazawa University, Kanazawa, pp. 13-36.

Glascock, M.D., 1999. An inter-laboratory comparison of element compositions for two obsidian sources. Int. Association for Obsidian Stud Bull. 23, 13–25.

Glascock, M.D., 2011. Comparison and contrast between XRF and NAA: used for characterization of obsidian sources in Central Mexico. In: Shackley, M.S. (Ed.), X-ray Fluorescence Spectrometry (XRF) in Geoarchaeology. Springer, pp. 161–192.

Glascock, M.D., Ferguson, J.R., 2012. Report on the Analysis of Obsidian Source Samples by Multiple Analytical Methods. Prepared for Bruce Kaiser, Bruker AXS, Kennewick, WA. Archaeometry Laboratory, University of Missouri Research Reactor Report.

Gratuze, B. 2007. Provenance study of obsidian artefacts found at three Chalcolithic and Bronze Age sites in Azerbaijan: KP408 (Kura river, north east of Akstafa), KP361 (north west of Ganja), KP 316 (north of Ganja). IRAMAT, Institut de Recherche sur les Archéomatériaux, Centre Ernest Babelon, C.N.R.S.

Gratuze, B., Barrandon, J.N., ISA, K.AL., Cauvin, M.C., 1993. Non-destructive analysis of obsidian artefacts using nuclear techniques: investigation of provenance of Near Eastern artefacts. Archaeometry 35 (1), 11–21.

Green, R.C., 1998. A 1990s Perspective on Method and Theory in Archaeological Volcanic Glass Studies. In: Shackley, M.S. (Ed.), Archaeological Obsidian Studies: Method and Theory. Plenum Press, New York, pp. 223–235.

Halama, R., Meliksetian, K., Savov, I.P., Sugden, P.J., Sokół, K., 2020. Pinched between the plates: Armenia's voluminous record of volcanic activity. Geol. Today 36, 101–108.

Hall, M.E., Shackley, M.S., 1994. An energy dispersive X-ray fluorescence study of some Near Eastern obsidians. Al-Rafidan 15, 25–32.

Hässig, M., Galoyan, G., Bruguier, O., Rolland, Y., Melis, R., Sosson, M. 2019. PTT history of the Amasia and Stepanavan sub-ophiolitic metamorphic units (NW Armenia, Lesser Caucasus): implications for metamorphic sole development and for the obduction process. Ofioliti: an international journal on ophiolites and related topics, 44(1), 43-70.

B.C. Hearn Jr. J.M. Donnelly-Nolan F.E. Goff Geologic map and structure sections of the Clear Lake Volcanics 1995 United States Geological Survey Northern California 10.3133/i2362.

Hughes, R.E., 1984. Obsidian Studies in the Great Basin. Contributions of the University of California Archaeological Research Facility, vol. 45. University of California.

Hughes, R.E., Smith, R.L. 1993. Archaeology, Geology, and Geochemistry of Obsidian Provenance Studies. In: Effects of Scale on Archaeological and Geological Perspectives, edited by J. K. Stein and A. R. Linse, pp. 79-91. GSA Special Paper. vol. 283. Geological Society of America, Boulder, Colorado.

Hunt, J., Hill, P., 2001. Tephrachronological Implications of Beam Size: Sample-Size Effects in Electron Microprobe Analysis of Glass Shards. J. Quat. Sci. 16 (2), 105–117.

Jackson, T.L., 1989. Late prehistoric obsidian production and exchange in the North Coast Ranges, California. In: Hughes, R.E. (Ed.), Current Directions in California Obsidian Studies, No. 48. Contributions of the University of California Archaeological Research Facility, pp. 79–94.

E. JAROSEWICH J.A. NELEN J.A. NORBERG Reference samples for electron microprobe analysis 4 1 1980 43 47.

Karapetian, K.I., Karapetian, S.G., 1971. Gegham volcanic highland. In: Mkrtchian, S.S. (Ed.), Late Orogenic Acid Volcanism of Armenian SSR: XV General Assembly of the International Geodetic and Geophysical Union Guide-Book of Excursions of the International Association of Volcanology and Chemistry of the Earth Interior. Acad. Sci. Arm. SSR, Yerevan, pp. 102–137.

Karapetian, S.G., 1966. Eruption centers of Pliocene acid rocks of Armenia. Volcanic And Volcano-Plutonic Formation. Nauka, Moscow, pp. 127–133.

Karapetian, S.G., 1968. About the age and stratigraphic position of recent rhyolite and rhyodacitic rocks of the Armenian SSR. Academy of Sciences of Armenian SSR. Earth Sci. XXI N1–2, 60–71.

Karapetian, S.G. 1970. Rhyolites and rhyodacites. Geology of SSR Armenia, vol. IV. Petrography. Volcanic rocks. Acad. Sci. SSR Armenia, Yerevan, pp. 604-638.

Karapetian, S.G., Jrbashian, R.T., Mnatsakanian, A.K., 2001. Late collision rhyolitic volcanism in the north-eastern part of the Armenian Highland. J. Volcanol. Geoth. Res. 112 (1–4), 189–220.

Keller, J., Djerbashian, E., Pernicka, E., Karapetian, S., Nasedkin, V. 1996. Armenian and Caucasian obsidian occurrences as sources for the Neolithic trade: volcanological setting and chemical characteristics. In: Archaeometry 94: The Proceedings of the 29th International Symposium on Archaeometry; Ankara, 914 May 1994, pp. 69–86.

Keller, J., Seifried, C., 1990. The present status of obsidian source identification in Anatolia and the Near East. PACT 25: Volcanology and archaeology. Proceedings of the European Workshops of Ravello. 25, 57–87.

Komarov, A.N., Skovorodkin, N.V., Karapetian, S.G., 1972. Determination of the age of natural glasses according to tracks of uranium fission fragments. Geochimia N6, 693–698.

Le Maitre, R.W., Streckeisen, A., Zanettin, B., Le Bas, M.J., Bonin, B., Bateman, P. (Eds.), 2002. Igneous Rocks: A Classification and Glossary of Terms: Recommendations of the International Union of Geological Sciences Subcommission on the Systematics of Igneous Rocks, 2nd ed. Cambridge University Press, Cambridge.

Lebedev, V.A., Chernyshev, I.V., Shatagin, K.N., Bubnov, S.N., Yakushev, A.I., 2013. The Quaternary volcanic rocks of the Geghama Highland, Lesser Caucasus, Armenia: geochronology, isotopic Sr-Nd characteristics, and origin. J. Volcanol. Seismol. 7, 204–229.

C.-M. Lin T.-L. Tseng K. Meliksetian A. Karakhanyan B.-S. Huang H. Babayan et al. Locally thin crust and high crustal VP/VS ratio beneath the Armenian volcanic highland of the Lesser Caucasus: A case for recent delamination. Journal of Geophysical Research: Solid Earth 125 2020 e2019JB019151.

K. Martirosyan-Olshansky Geochemical Characterization of Obsidian from the Neolithic Settlement Masis Blur, Ararat Plain, Armenia 2014 Austin, Texas.

Merrick, H.V., Brown, F.H., 1984a. Rapid chemical characterization of obsidian artifacts by electron microprobe analysis. Archaeometry 26, 230–236.

Merrick, H.V., Brown, F.H., 1984b. Obsidian sources and patterns of source utilization in Kenya and northern Tanzania: some initial findings. Afr. Archaeol. Rev. 2, 129–152.

Merrick, H.V., Brown, F.H., Nash, W.P., 1994. Use and movement of obsidian in the early and middle stone ages of Kenya and northern Tanzania. In: Childs, S.T. (Ed.), Society, Culture, and Technology in Africa. Masca Research Papers in Science and Archaeology, pp. 29-44.

Neff, H., 1998. Units in Chemistry-Based Ceramic Provenance Investigations. In: Ramenofsky, A.F., Steffen, A. (Eds.), Unit Issues in Archaeology: Measuring Time, Space, and Material. University of Utah Press, pp. 115–127.

Olshansky, K., 2018. Obsidian Economy in the Armenian Highlands During the Late Neolithic: A View from Masis Blur. PhD dissertation. Institute of Archaeology, University of California-Los Angeles.

Poidevin, J.-L., 1998. Les Gisements d'Obsidienne de Turquie et de Transcaucasie: Géologie, Géochimie et Chronomètrie. In: Cauvin, M.-.-C., Gourgaud, A., Gratauze, B., Arnaud, N., Poupeau, G., Poidevin, J.-.-L., Chataigner, C. (Eds.), L'obsidienne au Proche et Moyen-Orient: Du vVolcan à l'Outil. British Archaeological Reports. Archaeopress, Oxford, pp. 105–167.

Potts, P.J., Thompson, M., Wilson, S., Webb, P. 2005 G-Probe-2: An International Proficiency Test for Microbeam Laboratories - Report on Round 2 / May 2005 (NKT-1G Basaltic Glass).

Reed, W.P., 1992. Certificate: Standard Reference Material 278. Obsidian Rock, National Institute of Standards and Technology, Department of Commerce.

Reilinger, R.E., McClusky, S.C., Oral, M.B., King, R.W., Toksoz, M.N., Barka, A.A., Kinik, I., Lenk, O., Sanli, I., 1997. Global Positioning System measurements of present-day crustal movements in the Arabia-Africa-Eurasia plate collision zone. J. Geophys. Res.: Solid. Earth 102 (B5), 9983–9999.

Renfrew, C., Dixon, J., 1976. Obsidian in western Asia: a review. Probl. Econ. Soc. Archaeol. 42, 137–150.

Renfrew, C., Dixon, J., Cann, J., 1966. Obsidian and early cultural contact in the Near East. Proc. Prehist. Soc 2, 30–72.

Renfrew, C., Dixon, J., Cann, J., 1968. Further Analysis of Near Eastern Obsidians. Proc. Prehist. Soc 34, 319–331.

Shackley, M.S., 1988. Sources of archaeological obsidian in the Southwest: An archaeological, petrological, and geochemical study. Am. Antiq. 53, 752–772.

Shackley, M.S., 1995. Sources of Archaeological Obsidian in the Greater American Southwest: An Update and Quantitative Analysis. Am. Antiq. 60 (3), 531–551.

Shackley, M.S., 2005. Obsidian: Geology and Archaeology in the North American Southwest. University of Arizona.

Sherriff, J.E., Wilkinson, K.N., Adler, D.S., Arakelyan, D., Beverly, E.J., Blockley, S.P.E., Gasparyan, B., Mark, D.F., Meliksetian, K., Nahapetyan, S., Preece, K.J., Timms, R.G. O., 2019. Pleistocene volcanism and the geomorphological record of the Hrazdan valley, central Armenia: linking landscape dynamics and the Palaeolithic record. Quat. Sci. Rev. 226, 105994.

Shirinian, K.G., Karapetian, S.G., 1964. Specific features in the structure and petrology of rhyolithic dome-shaped volcanoes of Armenia. Bull. Volcanol. 27, 25–27.

Silva de la Mora, F.G., 2018. Obsidian procurement and distribution in the northwestern Maya lowlands during the Maya classic, a regional perspective. J. Archaeol. Sci. Rep. 18, 577–586.

Smith, D.B., 1995. Rhyolite, Glass Mountain RGM-1. Certificate of Analysis, United States Geological Survey.

Smith, H.W., Okazaki, R., Knowles, C.R., 1977. Electron microprobe data for tephra attributed to Glacier Peak. Washington. Quat. Res. 7, 197–206.

Sugden, P.J., Savov, I.P., Agostini, S., Wilson, M., Halama, R., Meliksetian, K.h., 2020. Boron isotope insights into the origin of subduction signatures in continent-continent collision zone volcanism. Earth Planet. Sci. Lett. 538, 116207.

Tryon, C., Logan, M., Mouralis, D., Kuhn, S., 2009. Building a tephrostratigraphic framework for the Paleolithic of central Anatolia. Turkey. J. Archaeol. Sci. 36, 637–652.

Tykot, R.H., 1997. Characterization of the Monte Arci (Sardinia) Obsidian Sources. J. Archaeol. Sci. 24 (5), 467–479.

Williams-Thorpe, O., 1995. Obsidian in the Mediterranean and the Near East: a provenancing success story. Archaeometry 37, 217–248.